
EGRU: Event-based GRU

for activity-sparse inference and learning

Anand Subramoney¹, Khaleelulla Khan Nazeer², Mark Schöne², Christian Mayr², David Kappel¹

¹ Institute for Neural Computation, Ruhr University Bochum, Germany

² Faculty of Electrical and Computer Engineering, Technische Universität Dresden, Dresden, Germany

{anand.subramoney,david.kappel}@ini.rub.de

{khaleelulla.khan_nazeer,mark.schoene,christian.mayr}@tu-dresden.de

Abstract

The scalability of recurrent neural networks (RNNs) is hindered by the sequential dependence of each time step’s computation on the previous time step’s output. Therefore, one way to speed up and scale RNNs is to reduce the computation required at each time step independent of model size and task. In this paper, we propose a model that reformulates Gated Recurrent Units (GRU) as an event-based activity-sparse model that we call the Event-based GRU (EGRU), where units compute updates only on receipt of input events (event-based) from other units. When combined with having only a small fraction of the units active at a time (activity-sparse), this model has the potential to be vastly more compute efficient than current RNNs. Notably, activity-sparsity in our model also translates into sparse parameter updates during gradient descent, extending this compute efficiency to the training phase. We show that the EGRU demonstrates competitive performance compared to state-of-the-art recurrent network models in real-world tasks, including language modeling while maintaining high activity sparsity naturally during inference and training. This sets the stage for the next generation of recurrent networks that are scalable and more suitable for novel neuromorphic hardware.

1 Introduction

Large scale models such as GPT-3 [6], switch transformers [15] and DALL-E [50] have demonstrated that scaling up deep learning models to billions of parameters cannot just improve the performance of these models but lead to entirely new forms of generalisation. For example, GPT-3 can do basic translation and addition even though it was trained only on next word prediction. While it is unknown if scaling up recurrent neural networks can lead to similar forms of generalisation, the limitations on scaling them up preclude studying this possibility. The dependence of each time step’s computation on the previous time step’s output is the source of a significant computational bottleneck, preventing RNNs from scaling well. Therefore, in recent years, RNNs, despite their many desirable theoretical properties [13] such as the ability to process much longer context and their computational power [55, 58], have been supplanted by feedforward network architectures.

By reducing the computation required at each time step, independent of model size and task, we can speed up and better scale RNNs. We propose to do this by designing a general-purpose event-based recurrent network architecture that is naturally activity-sparse. Dubbed the Event-based Gated Recurrent Unit (EGRU), our model is an extension of the Gated Recurrent Unit (GRU) [10]. With event-based communication, units in the model can decide when to send updates to other units, which then trigger the update of receiving units. Therefore, network updates are only performed at specific, dynamically determined event times. With activity-sparsity, most units do not send updates to other units most of the time, leading to substantial computational savings during training and inference. We formulate the gradient updates of the network to be sparse using a novel method, extending the benefit of the computational savings to training time.

The biological brain, which relies heavily on recurrent architectures and is at the same time extremely energy efficient [40], is a major source of inspiration for the EGRU. One of the brain’s strategies to reach these high levels of efficiency is activity-sparsity. In the brain, (asynchronous) event-based communication is just the result of the properties of the specific physical and biological substrate on which the brain is built. Biologically realistic spiking neural networks and neuromorphic hardware also aim to use these principles to build energy-efficient software and hardware models [51, 56]. However, despite progress in recent years, their task performance has been relatively limited for real-world tasks compared to state-of-the-art recurrent architectures based on LSTM and GRU. We view the EGRU as a generalisation of spiking neural networks, moving away from modeling biological dynamics toward a more general-purpose recurrent model for deep learning.

In this paper, we first introduce a version of EGRU based on a principled mathematical approach that formulates the dynamics of the internal states of the network in continuous time. The units of the network communicate solely through message events triggered when the internal state of a unit reaches a threshold value. This allows us to derive exact gradient descent update equations for the network analogous to backpropagation-through-time (BPTT) that mirrors the activity-sparsity of the forward pass.

We then introduce a discrete simplification of this continuous-time model that is also event-based and activity-sparse while being easier to implement on today’s prevailing machine learning libraries and thus directly comparable to existing implementations of GRU and LSTM. The backwards pass here uses an approximate version of BPTT, and these updates are also sparse.

In summary, the main contributions of this paper are the following:

1. We introduce the EGRU, an event-based continuous-time variant of the GRU model.
2. We derive an event-based form of the error-back-propagation algorithm for EGRU.
3. We introduce a discrete-time version of EGRU that can be directly compared to current LSTM/GRU implementations.
4. We demonstrate that the EGRU exhibits task-performance competitive with state-of-the-art recurrent network architectures (based on LSTM, GRU) on real-world machine learning benchmarks.
5. We show that EGRU exhibits high levels of activity-sparsity during both inference and learning.

We note here that methods for training with parameter sparsity or improving handling of long-term dependencies are both orthogonal to, and can be combined with our approach (which we plan to do in future work). Our focus, in this paper, is exclusively on using activity-sparsity to increase the efficiency of RNNs, specifically the GRU. We expect our method to be more efficient but not better at handling long-range dependencies compared to the GRU.

The sparsity of the backward-pass overcomes one of the major roadblocks in using large recurrent models, which is having enough computational resources to train them. We demonstrate the task performance and activity sparsity of the model implemented in PyTorch, but this formulation will also allow the model to run efficiently on off-the-shelf hardware, including CPU-based nodes when implemented using appropriate software paradigms. Moreover, an implementation on novel neuromorphic hardware like [11, 22], that is geared towards event-based computation, can make the model orders of magnitude more energy efficient [46].

2 Related work

Activity sparsity in RNNs has been proposed previously in various forms [23, 44, 45], but only focusing on achieving it during inference. Conditional computation is a form of activity sparsity used in [15] to scale to 1 trillion parameters. This architecture is based on the feedforward transformer architecture, with a separate network making the decision of which sub-networks should be active [57]. An asynchronous event-based architecture was recently proposed specifically targeted towards graph neural networks [54]. QRNNs [5], SRUs[34] and IndRNNs [35] target increasing the parallelism in a recurrent network without directly using activity-sparsity. Unlike [15], our architecture uses a unit-local decision making process for the dynamic activity-sparsity, specifically for recurrent architecture. The cost of computation is lower in an EGRU compared to [45], and can be implemented to have parallel computation of intermediate updates between events, while also being activity sparse in its output.

Models based on sparse communication [61] for scalability have been proposed recently for feedforward networks, using locality sensitivity hashing to dynamically choose downstream units for communicating activations. This is a dynamic form of parameter-sparsity [21]. But, parameter/model-sparsity is, in general, orthogonal to and complementary with our method for activity-sparsity, and can easily be combined for additional gains.

Biologically realistic spiking networks [38] are often implemented using event-based updates and have been scaled to huge sizes [28], albeit without any task-related performance evaluation. Models for deep learning with recurrent spiking networks [3, 53] mostly focus on modeling biologically realistic memory and learning mechanisms. Moreover, units in a spiking neural network implement dynamics based on biology and communicate solely through unitary events, while units in an EGRU send real-valued signals to other units, and have more general dynamics. A sparse learning rule was recently proposed [4] that is a local approximation of backpropagation through time, but not event-based.

The event-based learning rule for the continuous time EGRU is inspired by, and a generalization of, the event-prop learning rule for spiking neurons [60]. As in that paper, we use the adjoint method for ordinary differential equations (ODEs) to train the continuous time EGRU [8, 48] combined with sensitivity analysis for hybrid discrete/continuous systems [9, 16]. Using pseudo-derivatives for back-propagating through the non-differential threshold function, as we use for our discrete-time EGRU, was originally proposed for feedforward spiking networks in neuromorphic hardware in [14] and developed further in [3, 63]. The sparsity of learning with BPTT when using appropriate pseudo-derivatives in a discrete-time feed-forward spiking neural network was recently described in [47].

A continuous time version of sigmoidal RNNs was first proposed in [2] and for GRUs in [12]. The latter used a Bayesian update for network states when input events were received, but the network itself was not event-based. As in [33, 44], the focus there was on modeling irregularly spaced input data, and not on event-based network simulation or activity-sparse inference and training. [7] also recently proposed a continuous time recurrent network for more stable learning, without event-based mechanics. GRUs were formulated in continuous time in [27], but purely for analyzing its autonomous dynamics.

3 Event-based GRU

3.1 Time-spars GRU formulation

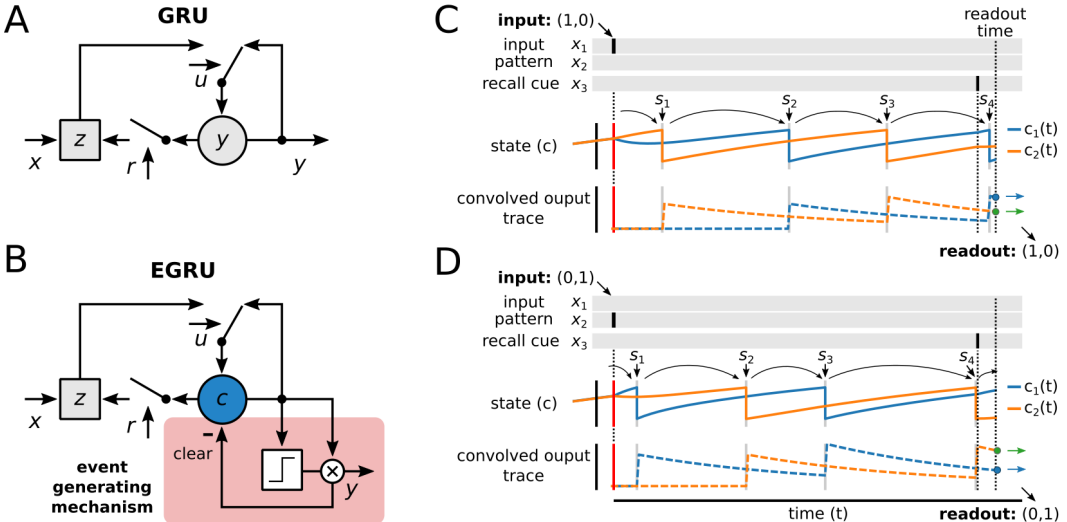


Figure 1: Illustration of EGRU. **A:** A single unit of the original GRU model adapted from [10]. **B:** EGRU unit with event generating mechanism. **C,D:** Dynamics of EGRU internal state variables for the delay-copy task with input (1,0) (C) and (0,1) (D). Colors are matched for neurons in both plots.

We base our model on the GRU [10], illustrated for convenience in Fig. 1A. It consists of internal gating variables for updates (u) and a reset (r), that determine the behavior of the internal state y . The state variable z determines the interaction between external input x and the internal state. The

dynamics of a layer of GRU units, at time step t , is given by the set of vector-valued update equations:

$$\begin{aligned} \mathbf{u}^{(t)} &= \sigma\left(\mathbf{W}_u \left[\mathbf{x}^{(t)}, \mathbf{y}^{(t-1)}\right] + \mathbf{b}_u\right), & \mathbf{r}^{(t)} &= \sigma\left(\mathbf{W}_r \left[\mathbf{x}^{(t)}, \mathbf{y}^{(t-1)}\right] + \mathbf{b}_r\right), \\ \mathbf{z}^{(t)} &= g\left(\mathbf{W}_z \left[\mathbf{x}^{(t)}, \mathbf{r}^{(t)} \odot \mathbf{y}^{(t-1)}\right] + \mathbf{b}_z\right), & \mathbf{y}^{(t)} &= \mathbf{u}^{(t)} \odot \mathbf{z}^{(t)} + (1 - \mathbf{u}^{(t)}) \odot \mathbf{y}^{(t-1)}, \end{aligned} \quad (1)$$

where $\mathbf{W}_{u/r/z}$, $\mathbf{b}_{u/r/z}$ denote network weights and biases, \odot denotes the element-wise (Hadamard) product, and $\sigma(\cdot)$ is the vectorized sigmoid function. The notation $[\mathbf{x}^{(t)}, \mathbf{y}^{(t-1)}]$ denotes vector concatenation. The function $g(\cdot)$ is an element-wise nonlinearity (typically the hyperbolic tangent function).

We introduce an event generating mechanisms by augmenting the GRU with a rectifier and a clearing mechanism (see Fig. 1B for an illustration). This introduces an event-based variant of the internal state variable $y_i^{(t)}$, that is nonzero when the internal dynamics reach a threshold ϑ_i and is cleared immediately afterwards. Formally, this can be included in the model by adding an auxiliary internal state $c_i^{(t)}$, and replacing $\mathbf{y}^{(t)} = (y_1^{(t)}, y_2^{(t)}, \dots)$ with the event-based form

$$y_i^{(t)} = c_i^{(t)} H\left(c_i^{(t)} - \vartheta_i\right) \quad \text{with} \quad c_i^{(t)} = u_i^{(t)} z_i^{(t)} + (1 - u_i^{(t)}) c_i^{(t-1)} - y_i^{(t-1)}, \quad (2)$$

where $H(\cdot)$ is the Heaviside step function and $\vartheta_i > 0$ is a trainable threshold parameter. This form is well suited for time sparsity, since $H(\cdot)$ acts here as a gating mechanism, by generating a single non-zero output when $c_i^{(t)}$ crosses the threshold ϑ_i . That is, at all time steps t with $c_i^{(t)} < \vartheta_i, \forall i$, we have $y_i^{(t)} = 0$. The $-y_i^{(t-1)}$ term in Eq. (2) makes emission of multiple consecutive events by the same unit unlikely, hence favoring overall sparse activity. With this formulation, each unit only needs to be updated when an input is received either externally or from another unit in the network. This is because, if both $x_i^{(t)} = y_i^{(t-1)} = 0$ for the i -th unit, then $u_i^{(t)}, r_i^{(t)}, z_i^{(t)}$ are essentially constants, and hence the update for $y_i^{(t)}$ can be retroactively calculated efficiently on the next incoming event.

3.2 Limit to continuous time

The discrete time model Eq. (1) considers the GRU dynamics only at integer time points, $t_0 = 0, t_1 = 1, t_2 = 2, \dots$. However, in general it is possible to express the GRU dynamics for an arbitrary time step Δt , with $t_n = t_{n-1} + \Delta t$. The discrete time GRU dynamics can be intuitively interpreted as an Euler discretization of an ordinary differential equation (ODE) [27] (see Supplement), which we extend further to formulate the EGRU. This is equivalent to taking the continuous time limit $\Delta t \rightarrow 0$ to get dynamics for the internal state $\mathbf{c}(t)$ starting from the discrete time EGRU model outlined above. In the resulting dynamical system equations inputs cause changes to the states only at the event times, whereas the dynamics between events can be expressed through ODEs. To arrive at the continuous time formulation we introduce the neuronal activations $\mathbf{a}_u(t)$, $\mathbf{a}_r(t)$ and $\mathbf{a}_z(t)$, with

$$\mathbf{u}(t) = \sigma(\mathbf{a}_u(t)), \quad \mathbf{r}(t) = \sigma(\mathbf{a}_r(t)), \quad \mathbf{z}(t) = g(\mathbf{a}_z(t)), \quad (3)$$

$$\text{with dynamics} \quad \tau_s \dot{\mathbf{a}}_x = -\mathbf{a}_x - \mathbf{b}_x, \quad \mathbf{x} \in \{u, r, z\}$$

and

$$\tau_m \dot{\mathbf{c}}(t) = \mathbf{u}(t) \odot (\mathbf{z}(t) - \mathbf{c}(t)) = F(t, \mathbf{a}_u, \mathbf{a}_r, \mathbf{a}_z, \mathbf{c}), \quad (4)$$

where τ_s and τ_m are time constants, $\mathbf{c}(t)$, $\mathbf{u}(t)$ and $\mathbf{z}(t)$ are the continuous time analogues to $\mathbf{c}^{(t)}$, $\mathbf{u}^{(t)}$ and $\mathbf{z}^{(t)}$, and $\dot{\mathbf{a}}_x$ denotes the time derivative of \mathbf{a}_x . The boundary conditions are defined for $t = 0$ as $\mathbf{a}_x(0) = \mathbf{c}(0) = \mathbf{0}$. The function F in Eq. (4) determines the behavior of the EGRU between event times, i.e. when $\mathbf{x}(t) = \mathbf{0}$ and $\mathbf{y}(t) = \mathbf{0}$. Nonzero external inputs and internal events cause jumps in $\mathbf{c}(t)$ and $\mathbf{a}_x(t)$.

Furthermore, the formulation of the event generating mechanisms Eq.(2) introduced above can be expressed in a straightforward manner in continuous time. Note that in continuous time the exact time s at which the internal variable $c_i(s)$ reaches the threshold ($c_i(s) = \vartheta_i$) can be determined with very high precision. Therefore, the value of $c_i(s)$ and the instantaneous amplitude of $y_i(s)$ simultaneously approach ϑ_i at time point s , so that the $-y_i$ term in Eq. (2) effectively resets $c_i(s)$ to zero, right after an event was triggered. To describe these dynamics we introduce the set of internal events \mathbf{e} , $e_k \in \mathbf{e}$,

$e_k = (s_k, n_k)$, where s_k are the continuous (real-valued) event times, and n_k denotes which unit got activated. An event e_k is triggered whenever $c_{n_k}(t)$ reaches ϑ . More precisely:

$$(s_k, n_k) : c_{n_k}^-(s_k) = \vartheta_{n_k}, \quad (5)$$

where the superscript \cdot^- (\cdot^+) denotes the quantity just before (after) the event. Immediately after an event has been generated the internal state is cleared: $c_{n_k}^+(s_k) = 0$. At the time of this event, the activations of all the units $m \neq n_k$ connected to unit n_k experiences a jump in its state value. The jump for $a_{X,m}$ is given by:

$$a_{X,m}^+(s_k) = a_{X,m}^-(s_k) + w_{X,mn_k} r_{X,n_k} c_{n_k}^-(s_k), \quad (6)$$

where $X \in \{u, r, z\}$, $\mathbf{r}_X = 1$ when $X \in \{u, z\}$ and $\mathbf{r}_X = \mathbf{r}$ when $X = \{r\}$. This is equivalent to $y_i = c_{n_k}^-$ being the output of each network unit. A similar jump is experienced on arrival of an external input, using the appropriate input weights instead (see Supplement for specifics).

The continuous time event-based state update is illustrated in Fig. 1C and D for the delay-copy task described in Section 4.1. Two EGRU units are used here and states $c_i(t)$ and event times s_k are shown. At the beginning of the trial an input pattern ($x_1 = 1$, $x_2 = 0$, and $x_1 = 0$, $x_2 = 1$ in Fig. 1C and D, respectively) has to be memorized in the network and retrieved again after the recall cue ($x_3 = 1$) was given. The parameters are trained with the event-based updates described in Section 3.3. The required memory is stored in the internal events and state dynamics. State updates can be performed in an event-based fashion, i.e. by jumping from one event time s_k to the next s_{k+1} . In-between state values follow the state dynamics Eq.(4) and their values are not needed to perform the updates (but are shown here for the sake of illustration). By construction, the state updates for external and internal events only happen on receipt of event. Since Eqs. (3), (4) are linear ODEs, the intermediate updates due to autonomous state dynamics can also be performed cumulatively and efficiently just at event times, hence avoiding any computation in the absence of incoming events.

3.3 Event-based gradient-descent using adjoint method

To derive the event-based gradient updates for the EGRU we define the loss over duration T as $\int_0^T \ell_c(\mathbf{c}(t), t) dt$, where $\ell_c(\mathbf{c}(t), t)$ is the instantaneous loss at time t . T is a task-specific time duration within which the training samples are given to the network as events, and the outputs are read out. In general $\ell_c(\mathbf{c}(t), t)$ may depend arbitrarily on $\mathbf{c}(t)$, however in practice we choose the instantaneous loss to depend on the EGRU states only at specific output times to adhere to our fully event-based algorithm.

The loss is augmented with the terms containing the Lagrange multipliers λ_c, λ_{a_x} to add constraints defining the dynamics of the system from Eqs. (3), (4). The total loss \mathcal{L} thus reads

$$\mathcal{L} = \int_0^T \left[\ell_c(\mathbf{c}(t), t) + \lambda_c \cdot (\tau_m \dot{\mathbf{c}}(t) - F(t, \mathbf{a}_u, \mathbf{a}_r, \mathbf{a}_z, \mathbf{c})) + \sum_{X \in \{u, r, z\}} \lambda_{a_x} \cdot (\tau_s \dot{\mathbf{a}}_X + \mathbf{a}_X) \right] dt. \quad (7)$$

The Lagrange multipliers are referred to as the adjoint variables in this context, and may be chosen freely since both $\tau_m \dot{\mathbf{c}}(t) - F(t, \mathbf{a}_u, \mathbf{a}_r, \mathbf{a}_z, \mathbf{c})$ and $\tau_s \dot{\mathbf{a}}_X + \mathbf{a}_X$ are everywhere zero by construction.

We can choose dynamics and jumps at events for the adjoint variables in such a way that they can be used to calculate the gradient $\frac{d\mathcal{L}}{dw_{ji}}$. Calculating the partial derivatives taking into account the discontinuous jumps at event times depends on the local application of the implicit function theorem, which requires event times to be a differentiable function of the parameters. See [8, 16, 60] for a description of applying the adjoint method for hybrid discrete/continuous time systems with further theoretical background, and the Supplement for a derivation specific to the EGRU.

The time dynamics of the adjoint variables is given by the following equations with a boundary condition of $\lambda_c(T) = \lambda_{a_x}(T) = 0$:

$$\left(\frac{\partial F}{\partial \mathbf{c}} \right)^T \lambda_c - \tau_m \dot{\lambda}_c = 0, \quad \lambda_{a_x} + \left(\frac{\partial F}{\partial \mathbf{a}_X} \right)^T \lambda_c - \tau_s \dot{\lambda}_{a_x} = 0, \quad (8)$$

for $X \in \{u, r, z\}$, and M^T denoting the transpose of the matrix M . The event updates for the adjoints are described in the Supplement. In practice, the integration of λ is done backwards in time.

For the recurrent weights $w_{x,ij}$ from the different parameter matrices W_x for $x \in u, r, z$, we can write the weight updates using only quantities calculated at events e_k as:

$$\Delta w_{x,ij} = \frac{\partial}{\partial w_{x,ij}} \mathcal{L}(\mathbf{W}) = \sum_k \xi_{x,ijk}. \quad (9)$$

The corresponding value of $\xi_{x,ijk} = (\xi_{x,k})_{ij}$ is given by the following formula, written in vector form for succinctness:

$$\xi_{x,k} = -\tau_s (\mathbf{r}_x^-(s_k) \odot \mathbf{c}^-(s_k)) \otimes \lambda_{a_x}^+(s_k), \quad (10)$$

where \otimes is the outer product, \mathbf{c}^- refers to the value of $\mathbf{c}(t)$ just before event e_k , $\mathbf{r}_x^- = 0$ for $x \in \{u, z\}$ and equal to the value of $\mathbf{r}(t)$ just before event e_k for $x = \{r\}$, $\lambda_{a_x}^+$ refers to the value of the adjoint variable $\lambda_{a_x}(t)$ just after the event e_k . Thus, the values of $\mathbf{r}(t), \mathbf{c}(t)$ needs to be stored only at event times, and $\lambda_{a_x}(t)$ needs to be calculated only at these times, making the gradient updates event-based. See the Supplement for the update rules for the input weights and biases.

3.4 Sparse approximate BPTT in discrete time

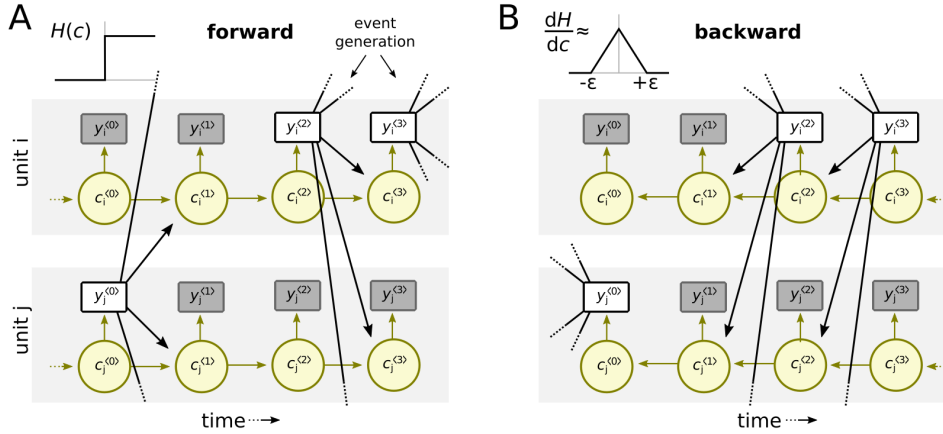


Figure 2: Illustrate the discrete time state dynamics for two EGRU units (i and j). **A:** Forward dynamics. Information only propagates from units that generate an event. **B:** Activity-sparse backward dynamics. Insets show threshold function $H(c)$ and pseudo derivative thereof.

In discrete time, the network uses a threshold activation function $H(c)$ to decide whether to emit an event as described in Eq. (2). Since $H(c)$ is not differentiable at the threshold ϑ_i , we define a pseudo-derivative at that point for calculating the backpropagated gradients. The pseudo-derivative is defined as a piecewise linear function that is non-zero for values of state c_i between $\vartheta_i + \varepsilon$ and $\vartheta_i - \varepsilon$ as shown in the inset in Fig. 2B. Since the pseudo-derivative is zero whenever the internal state of the unit is below $\vartheta_i - \varepsilon$, the backpropagated gradients are also 0 for all such units, making the backward-pass sparse (see Fig.2 for an illustration). Note that the case where the internal unit state is above $\vartheta_i + \varepsilon$ tends to occur less often, since the unit will emit an event and the internal state will be cleared (Eq. (2)) at the next simulation step.

3.5 Computation and memory reduction due to sparsity

For the forward pass of the discrete time EGRU, an activity sparsity of α (i.e. an average of α events per simulation step) leads to the reduction of multiply-accumulate operations (MAC), by factor α . We focus on MAC operations, since they are by far the most expensive compute operation in these models. If optimally implemented an activity sparsity of 80% will require 80% fewer MAC operations compared to a GRU that is not activity-sparse. Computation related to external input is only performed at input times, and hence is as sparse as the input, both in time and space. During the backward pass, a similar factor of computational reduction is observed, based on the backward-pass sparsity β which is, in general, less than α . This is because, when the internal state value is not within $\pm\varepsilon$ of the threshold ϑ , the backward pass is skipped, as described in section 3.4. Since our backward pass is also sparse, we expect to need to store only β fraction of the activations for later use, hence also reducing the memory usage. In all our experiments, we report activity-sparsity values calculated through simulations.

4 Results

4.1 Delay-copy task

To illustrate the behavior of the continuous-time EGRU model (Fig. 1C,D) we used a simple delay-copy task (also called the copy memory task [20]). A binary vector was presented to the network at the input time. This was followed by a delay period, after which the network was given a cue input indicating that it should recall the input seen before. A small network with only two EGRU units was used here, trained with the event-based learning rules described in Section 3.3. Right after the cue input, the network had to report the memorized input pattern. EGRU outputs y_i emitted at network event times were convolved with an exponential kernel to retrieve output traces, which were then used to retrieve the stored binary patterns based on their relative magnitudes. The kernel time constant was chosen to be significantly lower than the delay time such that the network had to retain the memory in the event dynamics. The binary cross-entropy loss was used to train this model until it reached perfect (100%) bitwise accuracy on this task. Fig. 1C,D shows the dynamics of the continuous-time model after training, as well as the output trace and events. The network has learned to generate events such that output traces reliably encode the stored input patterns. Supplemental Table S1 shows the robustness of the training for different sizes of inputs, networks, delay periods, all for multiple runs.

4.2 Gesture prediction

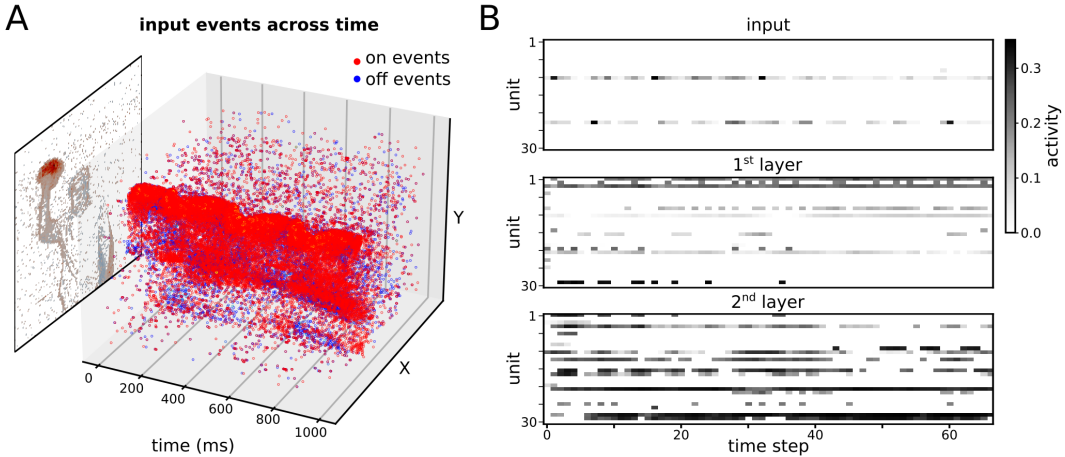


Figure 3: **A:** Illustration of DVS gesture classification data for an example class (right hand wave). On (red) and off (blue) events are shown over time and merged into a summary image for illustration (not presented to the network). **B:** Sparse activity of input and EGRU units (random subset of 30 units shown for each layer).

We evaluated our model on gesture prediction, which is a popular real-world benchmark for RNNs and widely used in neuromorphic research. The DVS128 Gesture Dataset [1], provides sparse event-based inputs which enables us to demonstrate our model’s performance and computational efficiency. The dataset contains 11 gestures from 29 subjects recorded with a DVS128 event camera [37]. Each event encodes a relative change of illumination and is given as spatio-temporal coordinates of X/Y position on the 128×128 -pixel sensor and time stamp. We combined the raw event times into ‘frames’ by binning them over time windows of 25 ms, and then downsampled them to 32×32 pixels using a maxpool layer.

Comparison of model performance on gesture prediction is presented in Table 1. The backward sparsity as described in Section 3.5 was calculated at epoch 100. EGRU consistently outperformed GRU networks of the same size on this task by a small margin. Adding data augmentation (DA) by applying random crop, translation, and rotation, as previously done in [25], increased the performance of pure RNN EGRU architecture to over 97%, coming close to state-of-the-art architectures without costly AlexNet pre-processing. We improved this result with a CNN feature extraction head adapted from AlexNet, DropConnect [59] applied to the hidden-to-hidden weights and Zoneout [31], outperforming [25] with far fewer parameters and an order of magnitude reduction in MAC operations. Further experimental details, ablation studies and statistics over different runs can be found in the supplement sections D.1, D.1.1 and tables S3, S6 respectively.

model	hidden dim	parameters	effective MAC	test accuracy	activity sparsity	backward sparsity
LSTM [19]	512	7.4 M	7.3 M	86.81%	-	-
AlexNet+LSTM+DA [25]	256	8.3 M	601.3 M	97.73%	-	-
GRU	1024	15.7 M	15.7 M	88.1%	0%	-
EGRU	512	5.5 M	4.2 M	88.0%	83.8%	46.8%
EGRU	1024	15.7 M	10.5 M	90.2%	82.5%	56.6%
EGRU+DA	1024	15.7 M	10.8 M	97.1%	78.8%	58.2%
CNN+EGRU+DA	256	2.7 M	79.6 M	97.3%	76.8%	56.9%
CNN+EGRU+DA	795	4.8 M	80.6 M	97.8%	76.4%	72.3%

Table 1: Model comparison for the DVS Gesture recognition task. Effective number of MAC operations as described in section 3.5. DA stands for Data Augmentation.

4.3 Sequential MNIST

We evaluated the EGRU on the sequential MNIST and permuted sequential MNIST tasks [32], which are widely used benchmarks for RNNs. In the sequential MNIST task, the MNIST handwritten digits were given as input one pixel at a time, and at the end of the input sequence, the network output was used to classify the digit. For the permuted sequential MNIST task, the pixels are permuted using a fixed permutation before being given as input in the same way. We trained a 1-layer EGRU with 590 units (matching the number of parameters with a 512 unit LSTM). We did not use any regularisation to increase sparsity in this task, so that we could test how much sparsity, both forward and backward, arises naturally in the EGRU.

In Table 2, we report the results of discrete-time EGRU along with other state-of-the-art architectures. EGRU achieved a task performance comparable to previous architectures while using much fewer operations (more than a 5-fold reduction in effective MAC operations compared to GRU). Further experimental details, and statistics over different runs can be found in the supplement sections D.2 and table S7 respectively.

dataset	model	hidden dim	parameters	effective MAC	test accuracy	activity sparsity	backward sparsity
sMNIST	coRNN [18]	256	134 K	262 K	99.4%	-	-
		512	1 M	1 M	98.9%	-	-
	GRU	590	1 M	1 M	98.8%	-	-
	EGRU	590	1 M	226 K	98.3%	72.1%	27.4%
psMNIST	coRNN [18]	256	134 K	262 K	97.3%	-	-
		512	1 M	1 M	95.1%	-	-
	EGRU	590	1 M	195 K	95.1%	82.0%	8.4%

Table 2: Model comparison on sequential MNIST (sMNIST) and permuted sequential MNIST (psMNIST) task. Top-1 test scores, given as percentage accuracy, where higher is better. coRNN is the model described in Rusch and Mishra [52].

4.4 Language Modeling

We evaluated our model on language modeling tasks based on the PennTreebank [39] dataset and the WikiText-2 dataset [42]. We focused exclusively on the RNN model in this work, and did not consider techniques such as neural cache models [17], Mixture-of-Softmaxes [62] or dynamic evaluation [30], all of which can be used on top of our model. A strong baseline for gate-based RNN architectures was established by [43]. Similarly, our models consisted of three stacked EGRU cells without skip connections. DropConnect [59] was applied to the hidden-to-hidden weights. The weights of the final softmax layer were tied to the embedding layer [24, 49]. All experimental details, and statistics over different runs can be found in the Supplement in sections D.3.1 and Table S8 respectively.

The results presented in Table 3 show that EGRU achieved performance competitive with AWD-LSTM [43]. At the same time, EGRU inherently exhibited activity sparsity that reduced the required computational operations (calculated analytically). Another desirable property of EGRU for resource constrained systems is a natural approach to model compression through pruning of least active units. We discuss our experimental findings for this pruning technique using language modeling as a case study in the Supplement (see Sec. D.4).

dataset	model	hidden dim	parameters	effective MAC	test	activity sparsity	backward sparsity
PTB	Merity et al. [43]	1150	24 M	24.0 M	57.3	-	-
	Li et al. [36]	-	52 M	51.6 M	55.2	-	-
	GRU	1350	28 M	27.6 M	66.3	-	-
	EGRU	1350	33 M	9.9 M	57.2	79.7%	46.3%
	EGRU	2000	55 M	12.7 M	57.0	84.8%	42.9%
	[41]	-	24 M	-	65.9	-	-
WikiText-2	[43]	1150	33 M	32.0 M	65.8	-	-
	GRU	1350	39 M	38.8 M	71.8	-	-
	EGRU	1350	51 M	17.5 M	70.6	76.8 %	44.2 %
	EGRU	2000	74 M	20.1 M	68.9	82.7 %	42.2 %

Table 3: Model comparison on PennTreebank and WikiText-2. Test scores are given as perplexities, where lower is better. Effective MAC operations are given for a single time step and consider the layer-wise sparsity in the forward pass. Activity sparsity is given for the trained model to resemble inference sparsity. Backward sparsity is averaged over the whole training. Model parameters were optimized on Penn Treebank and transferred to WikiText-2.

5 Discussion

We have introduced EGRU, a new form of a recurrent neural network that is competitive with current deep recurrent models yet can efficiently perform both inference and learning. To achieve this, we first formulated the GRU in continuous time and converted it to an event-based form that achieved activity-sparsity naturally. Furthermore, the gradient-descent updates on this time-continuous EGRU mirrored the activity sparsity of the inference. We then demonstrated a discrete-time simplification of this model that also exhibited event-based activity-sparse inference and learning while being easier to implement with popular ML frameworks such as PyTorch or Tensorflow.

The EGRU achieved competitive task performance on various real-world tasks such as gesture recognition and language modeling while achieving a sparsity of up to 80% for the gesture recognition task and 90% on the language modeling task. Scaling up networks for language modeling has shown some of the most promising results in the last few years [6, 15] Hence our choice of task, albeit on a smaller scale, was to validate the functionality of the model. Considering the need for extensive hyperparameter search [41] for language modeling, our model achieved promising results while maintaining a high degree of activity-sparsity. For example, our EGRU with 1350 hidden units reached perplexities comparable with LSTM and GRU, while maintaining an activity-sparsity of 86 % (14% of the units active on average). The amount of computation used by an EGRU also scales sub-linearly with an increase in the size of the network and number of parameters, making it a scalable alternative to LSTM/GRU based architectures (see Supplement).

While we use the GRU as the basis for our model due to its simplicity, this formulation can easily be extended to any arbitrary network dynamics, including the LSTM, allowing specialized architectures for different domains. The adjoint method for hybrid systems that we use here is a powerful general-purpose tool for training event-based activity-sparse forms of various recurrent neural network architectures. Another novel outcome of this paper is that this theory can handle inputs in continuous time as events, which is very intuitive, hence providing an alternative to the more complex controlled differential equations [29]. The EGRU can also be used for irregularly spaced sequential data quite naturally.

The compute efficiency of this model can directly translate into gains in energy efficiency when implemented using event-based software primitives. These same properties would also allow the

model to work well on heterogenous compute resources, including pure CPU nodes, and neuromorphic devices such as Intel’s Loihi [11] and SpiNNaker 2 [22], that can achieve orders of magnitude higher energy efficiency. The EGRU model will also perform well in more mainstream deep learning hardware that is enabled for dynamic sparsity, such as the Graphcore system [26]. On neuromorphic devices with on-chip memory in the form of a crossbar array, the activity sparsity directly translates into energy efficiency. For larger models that need off-chip memory, activity-sparsity needs to be combined with parameter-sparsity to reduce energy-intensive memory access operations.

In summary, starting with the motivation of building scalable, energy-efficient deep recurrent models, we demonstrated the EGRU, which reduces the required compute for both inference and learning by enhancing sparsity in the network. This approach lays the foundation for exploring novel capabilities that can emerge from scaling up RNNs similar to what has been seen for feed-forward architectures in recent years.

6 Acknowledgements

The authors gratefully acknowledge the GWK support for funding this project by providing computing time through the Center for Information Services and HPC (ZIH) at TU Dresden. We acknowledge the use of Fenix Infrastructure resources, which are partially funded from the European Union’s Horizon 2020 research and innovation programme through the ICEI project under the grant agreement No. 800858. AS is funded by the Ministry of Culture and Science of the State of North Rhine-Westphalia, Germany. KKN is funded by the German Federal Ministry of Education and Research (BMBF) within the KI-ASIC project (16ES0996). MS is fully funded by a grant of the Bosch Research Foundation. The authors would like to thank Darjan Salaj, Melika Payvand, Markus Murschitz, Franz Scherr, Robin Schiewer for helpful comments on this manuscript. AS would also like to thank Darjan Salaj and Franz Scherr for insightful early discussions.

References

- [1] A. Amir, B. Taba, D. Berg, T. Melano, J. McKinstry, C. Di Nolfo, T. Nayak, A. Andreopoulos, G. Garreau, M. Mendoza, et al. A low power, fully event-based gesture recognition system. In *Proceedings of the IEEE conference on computer vision and pattern recognition*, pages 7243–7252, 2017.
- [2] R. D. Beer. On the Dynamics of Small Continuous-Time Recurrent Neural Networks. *Adaptive Behavior*, 3(4):469–509, Mar. 1995. ISSN 1059-7123. doi: 10.1177/105971239500300405.
- [3] G. Bellec, D. Salaj, A. Subramoney, R. Legenstein, and W. Maass. Long short-term memory and Learning-to-learn in networks of spiking neurons. In S. Bengio, H. Wallach, H. Larochelle, K. Grauman, N. Cesa-Bianchi, and R. Garnett, editors, *Advances in Neural Information Processing Systems 31*, pages 787–797. Curran Associates, Inc., 2018.
- [4] G. Bellec, F. Scherr, A. Subramoney, E. Hajek, D. Salaj, R. Legenstein, and W. Maass. A solution to the learning dilemma for recurrent networks of spiking neurons. *Nature Communications*, 11(1):3625, July 2020. ISSN 2041-1723. doi: 10.1038/s41467-020-17236-y.
- [5] J. Bradbury, S. Merity, C. Xiong, and R. Socher. Quasi-Recurrent Neural Networks. *arXiv:1611.01576 [cs]*, Nov. 2016.
- [6] T. B. Brown, B. Mann, N. Ryder, M. Subbiah, J. Kaplan, P. Dhariwal, A. Neelakantan, P. Shyam, G. Sastry, A. Askell, S. Agarwal, A. Herbert-Voss, G. Krueger, T. Henighan, R. Child, A. Ramesh, D. M. Ziegler, J. Wu, C. Winter, C. Hesse, M. Chen, E. Sigler, M. Litwin, S. Gray, B. Chess, J. Clark, C. Berner, S. McCandlish, A. Radford, I. Sutskever, and D. Amodei. Language Models are Few-Shot Learners. *arXiv:2005.14165 [cs]*, July 2020.
- [7] B. Chang, M. Chen, E. Haber, and E. H. Chi. AntisymmetricRNN: A Dynamical System View on Recurrent Neural Networks. *arXiv:1902.09689 [cs, stat]*, Feb. 2019.
- [8] R. T. Q. Chen, Y. Rubanova, J. Bettencourt, and D. K. Duvenaud. Neural Ordinary Differential Equations. In S. Bengio, H. Wallach, H. Larochelle, K. Grauman, N. Cesa-Bianchi, and R. Garnett, editors, *Advances in Neural Information Processing Systems 31*, pages 6572–6583. Curran Associates, Inc., 2018.

- [9] R. T. Q. Chen, B. Amos, and M. Nickel. Learning Neural Event Functions for Ordinary Differential Equations. In *International Conference on Learning Representations*, Sept. 2020. URL https://openreview.net/forum?id=kW_zpEmMLdP.
- [10] K. Cho, B. Van Merriënboer, C. Gulcehre, D. Bahdanau, F. Bougares, H. Schwenk, and Y. Bengio. Learning phrase representations using rnn encoder-decoder for statistical machine translation. *arXiv preprint arXiv:1406.1078*, 2014.
- [11] M. Davies, N. Srinivasa, T.-H. Lin, G. China, Y. Cao, S. H. Choday, G. Dimou, P. Joshi, N. Imam, S. Jain, et al. Loihi: A neuromorphic manycore processor with on-chip learning. *Ieee Micro*, 38(1):82–99, 2018.
- [12] E. De Brouwer, J. Simm, A. Arany, and Y. Moreau. GRU-ODE-Bayes: Continuous Modeling of Sporadically-Observed Time Series. In *Advances in Neural Information Processing Systems*, volume 32. Curran Associates, Inc., 2019. URL <https://proceedings.neurips.cc/paper/2019/hash/455cb2657aaa59e32fad80cb0b65b9dc-Abstract.html>.
- [13] M. Dehghani, S. Gouws, O. Vinyals, J. Uszkoreit, and L. Kaiser. Universal Transformers. In *International Conference on Learning Representations*, Sept. 2018. URL <https://openreview.net/forum?id=HyzdRiR9Y7¬eId=HyxfZDmCk4¬eId=rkginvfklN>.
- [14] S. K. Esser, P. A. Merolla, J. V. Arthur, A. S. Cassidy, R. Appuswamy, A. Andreopoulos, D. J. Berg, J. L. McKinstry, T. Melano, D. R. Barch, C. di Nolfo, P. Datta, A. Amir, B. Taba, M. D. Flickner, and D. S. Modha. Convolutional networks for fast, energy-efficient neuromorphic computing. *Proceedings of the National Academy of Sciences*, 113(41):11441–11446, Nov. 2016. ISSN 0027-8424, 1091-6490. doi: 10.1073/pnas.1604850113. URL <http://www.pnas.org/content/113/41/11441>.
- [15] W. Fedus, B. Zoph, and N. Shazeer. Switch Transformers: Scaling to Trillion Parameter Models with Simple and Efficient Sparsity. *arXiv:2101.03961 [cs]*, Jan. 2021.
- [16] S. Galán, W. F. Feehery, and P. I. Barton. Parametric sensitivity functions for hybrid discrete/continuous systems. *Applied Numerical Mathematics*, 31(1):17–47, Sept. 1999. ISSN 0168-9274. doi: 10.1016/S0168-9274(98)00125-1.
- [17] E. Grave, A. Joulin, and N. Usunier. Improving neural language models with a continuous cache. In *5th International Conference on Learning Representations, ICLR 2017, Toulon, France, April 24-26, 2017, Conference Track Proceedings*. OpenReview.net, 2017. URL <https://openreview.net/forum?id=B184E5qee>.
- [18] A. Gu, C. Gulcehre, T. Paine, M. Hoffman, and R. Pascanu. Improving the Gating Mechanism of Recurrent Neural Networks. In *Proceedings of the 37th International Conference on Machine Learning*, pages 3800–3809. PMLR, Nov. 2020. URL <https://proceedings.mlr.press/v119/gu20a.html>.
- [19] W. He, Y. Wu, L. Deng, G. Li, H. Wang, Y. Tian, W. Ding, W. Wang, and Y. Xie. Comparing snns and rnns on neuromorphic vision datasets: Similarities and differences. *Neural Networks*, 132:108–120, 2020.
- [20] S. Hochreiter and J. Schmidhuber. Long Short-Term Memory. *Neural Computation*, 9(8):1735–1780, Nov. 1997. ISSN 0899-7667. doi: 10.1162/neco.1997.9.8.1735.
- [21] T. Hoefler, D. Alistarh, T. Ben-Nun, N. Dryden, and A. Peste. Sparsity in deep learning: Pruning and growth for efficient inference and training in neural networks. *Journal of Machine Learning Research*, 22(241):1–124, 2021.
- [22] S. Höppner, Y. Yan, B. Vogginger, A. Dixius, J. Partzsch, F. Neumärker, S. Hartmann, S. Schiefer, S. Scholze, G. Ellguth, et al. Dynamic voltage and frequency scaling for neuromorphic many-core systems. In *2017 IEEE International Symposium on Circuits and Systems (ISCAS)*, pages 1–4. IEEE, 2017.
- [23] K. L. Hunter, L. Spracklen, and S. Ahmad. Two sparsities are better than one: Unlocking the performance benefits of sparse-sparse networks, 2021.

- [24] H. Inan, K. Khosravi, and R. Socher. Tying word vectors and word classifiers: A loss framework for language modeling. In *5th International Conference on Learning Representations, ICLR 2017, Toulon, France, April 24-26, 2017, Conference Track Proceedings*. OpenReview.net, 2017. URL <https://openreview.net/forum?id=r1aPbsFle>.
- [25] S. U. Innocenti, F. Becattini, F. Pernici, and A. Del Bimbo. Temporal binary representation for event-based action recognition. In *2020 25th International Conference on Pattern Recognition (ICPR)*, pages 10426–10432. IEEE, 2021.
- [26] Z. Jia, B. Tillman, M. Maggioni, and D. P. Scarpazza. Dissecting the graphcore ipu architecture via microbenchmarking. *arXiv preprint arXiv:1912.03413*, 2019.
- [27] I. D. Jordan, P. A. Sokół, and I. M. Park. Gated recurrent units viewed through the lens of continuous time dynamical systems. *Frontiers in computational neuroscience*, page 67, 2021.
- [28] J. Jordan, T. Ippen, M. Helias, I. Kitayama, M. Sato, J. Igarashi, M. Diesmann, and S. Kunkel. Extremely Scalable Spiking Neuronal Network Simulation Code: From Laptops to Exascale Computers. *Frontiers in Neuroinformatics*, 12:2, 2018. ISSN 1662-5196.
- [29] P. Kidger, J. Morrill, J. Foster, and T. Lyons. Neural controlled differential equations for irregular time series. *Advances in Neural Information Processing Systems*, 33:6696–6707, 2020.
- [30] B. Krause, E. Kahembwe, I. Murray, and S. Renals. Dynamic evaluation of neural sequence models. In J. Dy and A. Krause, editors, *Proceedings of the 35th International Conference on Machine Learning*, volume 80 of *Proceedings of Machine Learning Research*, pages 2766–2775. PMLR, 10–15 Jul 2018. URL <https://proceedings.mlr.press/v80/krause18a.html>.
- [31] D. Krueger, T. Maharaj, J. Kramár, M. Pezeshki, N. Ballas, N. R. Ke, A. Goyal, Y. Bengio, A. Courville, and C. Pal. Zoneout: Regularizing rnns by randomly preserving hidden activations, 2016. URL <https://arxiv.org/abs/1606.01305>.
- [32] Q. V. Le, N. Jaitly, and G. E. Hinton. A simple way to initialize recurrent networks of rectified linear units. *arXiv preprint arXiv:1504.00941*, 2015.
- [33] M. Lechner and R. Hasani. Learning Long-Term Dependencies in Irregularly-Sampled Time Series. *arXiv:2006.04418 [cs, stat]*, Dec. 2020. URL <http://arxiv.org/abs/2006.04418>.
- [34] T. Lei, Y. Zhang, S. I. Wang, H. Dai, and Y. Artzi. Simple Recurrent Units for Highly Parallelizable Recurrence. *arXiv:1709.02755 [cs]*, Sept. 2017.
- [35] S. Li, W. Li, C. Cook, C. Zhu, and Y. Gao. Independently Recurrent Neural Network (IndRNN): Building A Longer and Deeper RNN. *arXiv:1803.04831 [cs]*, May 2018.
- [36] S. Li, W. Li, C. Cook, Y. Gao, and C. Zhu. Deep independently recurrent neural network (indrnn). *CoRR*, abs/1910.06251, 2019. URL <http://arxiv.org/abs/1910.06251>.
- [37] P. Lichtsteiner, C. Posch, and T. Delbruck. A 128×128 120 dB 15 μ s latency asynchronous temporal contrast vision sensor. *IEEE journal of solid-state circuits*, 43(2):566–576, 2008.
- [38] W. Maass. Networks of spiking neurons: the third generation of neural network models. *Neural networks*, 10(9):1659–1671, 1997.
- [39] M. P. Marcus, M. A. Marcinkiewicz, and B. Santorini. Building a large annotated corpus of english: The penn treebank. *Comput. Linguist.*, 19(2):313–330, jun 1993. ISSN 0891-2017.
- [40] C. Mead. How we created neuromorphic engineering. *Nature Electronics*, 3(7):434–435, 2020.
- [41] G. Melis, C. Dyer, and P. Blunsom. On the state of the art of evaluation in neural language models. In *6th International Conference on Learning Representations, ICLR 2018, Vancouver, BC, Canada, April 30 - May 3, 2018, Conference Track Proceedings*. OpenReview.net, 2018. URL <https://openreview.net/forum?id=ByJHuTgA->.
- [42] S. Merity, C. Xiong, J. Bradbury, and R. Socher. Pointer sentinel mixture models, 2016. URL <https://arxiv.org/abs/1609.07843>.

- [43] S. Merity, N. S. Keskar, and R. Socher. Regularizing and Optimizing LSTM Language Models. *arXiv:1708.02182 [cs]*, Aug. 2017.
- [44] D. Neil, M. Pfeiffer, and S.-C. Liu. Phased LSTM: Accelerating Recurrent Network Training for Long or Event-based Sequences. *arXiv:1610.09513 [cs]*, Oct. 2016.
- [45] D. Neil, J. H. Lee, T. Delbruck, and S.-C. Liu. Delta Networks for Optimized Recurrent Network Computation. In *International Conference on Machine Learning*, pages 2584–2593. PMLR, July 2017.
- [46] C. Ostrau, C. Klarhorst, M. Thies, and U. Rückert. Benchmarking neuromorphic hardware and its energy expenditure. *Frontiers in neuroscience*, 16, 2022.
- [47] N. Perez-Nieves and D. F. M. Goodman. Sparse Spiking Gradient Descent. *arXiv:2105.08810 [cs, q-bio]*, May 2021.
- [48] L. Pontryagin, V. Boltyanskiy, R. V. Gamkrelidze, and Y. MISHCHENKO. *Mathematical theory of optimal processes*. CRC press, 1962.
- [49] O. Press and L. Wolf. Using the output embedding to improve language models. In *Proceedings of the 15th Conference of the European Chapter of the Association for Computational Linguistics: Volume 2, Short Papers*, pages 157–163, Valencia, Spain, Apr. 2017. Association for Computational Linguistics. URL <https://aclanthology.org/E17-2025>.
- [50] A. Ramesh, M. Pavlov, G. Goh, S. Gray, C. Voss, A. Radford, M. Chen, and I. Sutskever. Zero-Shot Text-to-Image Generation. *arXiv:2102.12092 [cs]*, Feb. 2021.
- [51] K. Roy, A. Jaiswal, and P. Panda. Towards spike-based machine intelligence with neuromorphic computing. *Nature*, 575(7784):607–617, 2019.
- [52] T. K. Rusch and S. Mishra. Coupled Oscillatory Recurrent Neural Network (coRNN): An accurate and (gradient) stable architecture for learning long time dependencies. *arXiv:2010.00951 [cs, stat]*, Mar. 2021. URL <http://arxiv.org/abs/2010.00951>.
- [53] D. Salaj, A. Subramoney, C. Krausnikovic, G. Bellec, R. Legenstein, and W. Maass. Spike frequency adaptation supports network computations on temporally dispersed information. *eLife*, 10:e65459, July 2021. ISSN 2050-084X. doi: 10.7554/eLife.65459. URL <https://doi.org/10.7554/eLife.65459>.
- [54] S. Schaefer, D. Gehrig, and D. Scaramuzza. Aegnn: Asynchronous event-based graph neural networks. *arXiv preprint arXiv:2203.17149*, 2022.
- [55] A. M. Schäfer and H. G. Zimmermann. Recurrent Neural Networks Are Universal Approximators. In S. D. Kollias, A. Stafylopatis, W. Duch, and E. Oja, editors, *Artificial Neural Networks – ICANN 2006*, Lecture Notes in Computer Science, pages 632–640, Berlin, Heidelberg, 2006. Springer. ISBN 978-3-540-38627-8. doi: 10.1007/11840817_66.
- [56] C. D. Schuman, T. E. Potok, R. M. Patton, J. D. Birdwell, M. E. Dean, G. S. Rose, and J. S. Plank. A survey of neuromorphic computing and neural networks in hardware. *arXiv preprint arXiv:1705.06963*, 2017.
- [57] N. Shazeer, A. Mirhoseini, K. Maziarz, A. Davis, Q. Le, G. Hinton, and J. Dean. Outrageously Large Neural Networks: The Sparsely-Gated Mixture-of-Experts Layer. *arXiv:1701.06538 [cs, stat]*, Jan. 2017.
- [58] H. T. Siegelmann and E. D. Sontag. On the Computational Power of Neural Nets. *Journal of Computer and System Sciences*, 50(1):132–150, Feb. 1995. ISSN 0022-0000. doi: 10.1006/jcss.1995.1013. URL <http://www.sciencedirect.com/science/article/pii/S0022000085710136>.
- [59] L. Wan, M. Zeiler, S. Zhang, Y. Le Cun, and R. Fergus. Regularization of neural networks using dropout. In S. Dasgupta and D. McAllester, editors, *Proceedings of the 30th International Conference on Machine Learning*, volume 28 of *Proceedings of Machine Learning Research*, pages 1058–1066, Atlanta, Georgia, USA, 17–19 Jun 2013. PMLR. URL <https://proceedings.mlr.press/v28/wan13.html>.

- [60] T. C. Wunderlich and C. Pehle. Event-based backpropagation can compute exact gradients for spiking neural networks. *Scientific Reports*, 11(1):12829, June 2021. ISSN 2045-2322. doi: 10.1038/s41598-021-91786-z. URL <https://www.nature.com/articles/s41598-021-91786-z>.
- [61] M. Yan, N. Meisburger, T. Medini, and A. Shrivastava. Distributed slide: Enabling training large neural networks on low bandwidth and simple cpu-clusters via model parallelism and sparsity. *arXiv preprint arXiv:2201.12667*, 2022.
- [62] Z. Yang, Z. Dai, R. Salakhutdinov, and W. W. Cohen. Breaking the softmax bottleneck: A high-rank RNN language model. In *International Conference on Learning Representations*, 2018. URL <https://openreview.net/forum?id=HkwZSG-CZ>.
- [63] F. Zenke and S. Ganguli. SuperSpike: Supervised Learning in Multilayer Spiking Neural Networks. *Neural Computation*, 30(6):1514–1541, Apr. 2018. ISSN 0899-7667. doi: 10.1162/neco_a_01086. URL https://doi.org/10.1162/neco_a_01086.

Supplementary information “EGRU: Event-based GRU for activity-sparse inference and learning”

Anand Subramoney¹, Khaleelulla Khan Nazeer², Mark Schöne², Christian Mayr², David Kappel¹

¹ Institute for Neural Computation, Ruhr University Bochum, Germany

² Faculty of Electrical and Computer Engineering, Technische Universität Dresden, Dresden, Germany

{anand.subramoney,david.kappel}@ini.rub.de

{khaleelulla.khan_nazeer,mark.schoene,christian.mayr}@tu-dresden.de

A Derivation of continuous time version of GRU

In this section we derive the continuous-time version of the GRU model. Note that our definition of the GRU differs from the original version, presented in [4], by inverting the role of the $\mathbf{u}^{(t)}$ and $1 - \mathbf{u}^{(t)}$ terms in the updates equations for $\mathbf{y}^{(t)}$ (a change in sign). This substitution does not change the behavior of the model but simplifies the notation in the continuous-time version of the model.

We first rewrite the dynamics of a layer of GRU units at time step t from Eq. (1) of the main text, separating out the input and recurrent weights:

$$\begin{aligned} \mathbf{u}^{(t)} &= \sigma \left(\mathbf{U}_u \mathbf{x}^{(t)} + \mathbf{V}_u \mathbf{y}^{(t-1)} + \mathbf{b}_u \right), \quad \mathbf{r}^{(t)} = \sigma \left(\mathbf{U}_r \mathbf{x}^{(t)} + \mathbf{V}_r \mathbf{y}^{(t-1)} + \mathbf{b}_r \right), \\ \mathbf{z}^{(t)} &= g \left(\mathbf{U}_z \mathbf{x}^{(t)} + \mathbf{V}_z \left(\mathbf{r}^{(t)} \odot \mathbf{y}^{(t-1)} \right) + \mathbf{b}_z \right), \quad \mathbf{y}^{(t)} = \mathbf{u}^{(t)} \odot \mathbf{z}^{(t)} + (1 - \mathbf{u}^{(t)}) \odot \mathbf{y}^{(t-1)}, \end{aligned} \quad (\text{S1})$$

we can write this as

$$\mathbf{y}^{(t)} - \mathbf{y}^{(t-1)} = -\mathbf{u}^{(t)} \odot \mathbf{y}^{(t-1)} + \mathbf{u}^{(t)} \odot \mathbf{z}^{(t)}. \quad (\text{S2})$$

Note that \mathbf{u} here is equivalent to $\tilde{\mathbf{u}} = 1 - \mathbf{u}$ used in the standard GRU model. Eq. (S2) is in the form of a forward Euler discretization of a continuous time dynamical system. Defining $\mathbf{y}(t) \equiv \mathbf{y}^{(t-1)}$, we get $\mathbf{r}(t) \equiv \mathbf{r}^{(t)}$, $\mathbf{u}(t) \equiv \mathbf{u}^{(t)}$, $\mathbf{z}(t) \equiv \mathbf{z}^{(t)}$. Let Δt define an arbitrary time step. Then Eq. (S2) becomes:

$$\mathbf{y}(t + \Delta t) - \mathbf{y}(t) = -\mathbf{u}(t) \odot (\mathbf{y}(t) + \mathbf{z}(t)) \Delta t \quad (\text{S3})$$

Dividing by Δt and taking limit $\Delta t \rightarrow 0$, we get:

$$\dot{\mathbf{y}}(t) = -\mathbf{u}(t) \odot (\mathbf{y}(t) - \mathbf{z}(t)), \quad (\text{S4})$$

where $\dot{\mathbf{y}}(t) \equiv \frac{d\mathbf{y}(t)}{dt}$ is the time derivative of $\mathbf{y}(t)$.

B Full details of the continuous time EGRU

In this section we establish the continuous time version of the EGRU model. To describe the event generating mechanism and state dynamics it is convenient to express the dynamical system equations in terms of the activations \mathbf{a}_x .

We first rewrite Eqs. (3) & (4) of the main text, as:

$$f_{a_x} \equiv \tau_s \dot{\mathbf{a}}_x + \mathbf{a}_x + \mathbf{b}_x = \mathbf{0}, \quad x \in \{u, r, z\} \quad (\text{S5})$$

$$f_c \equiv \tau_m \dot{\mathbf{c}}(t) + \mathbf{u}(t) \odot (\mathbf{c}(t) - \mathbf{z}(t)) = \tau_m \dot{\mathbf{c}}(t) - F(t, \mathbf{a}_u, \mathbf{a}_r, \mathbf{a}_z, \mathbf{c}) = 0. \quad (\text{S6})$$

We write the event transitions for \mathbf{c} at network event $e_k \in \mathbf{e}$, $e_k = (s_k, n_k)$, where s_k are the continuous (real-valued) event times, and n_k denotes which unit got activated, and using the superscript \cdot^- (\cdot^+) to the quantity just before (after) the event, as:

$$c_{n_k}^-(s_k) = \vartheta_{n_k}, \quad c_{n_k}^+(s_k) = 0, \quad c_m^+(s_k) = c_m^-(s_k). \quad (\text{S7})$$

where $m \neq n_k$ denotes all the units connected to unit n_k that are not activated. At the time of this event, the activations $a_{X,m}$ ($X \in \{u, r, x\}$) experiences a jump in its state value, given by:

$$a_{u,m}^+(s_k) = a_{u,m}^-(s_k) + v_{u,mn_k} \times c_{n_k}^-(s_k), \quad (\text{S8})$$

$$a_{r,m}^+(s_k) = a_{r,m}^-(s_k) + v_{r,mn_k} \times c_{n_k}^-(s_k), \quad (\text{S9})$$

$$a_{z,m}^+(s_k) = a_{z,m}^-(s_k) + v_{z,mn_k} \times r_{n_k} \times c_{n_k}^-(s_k), \quad (\text{S10})$$

$$a_{X,n_k}^+(s_k) = a_{X,n_k}^-(s_k). \quad (\text{S11})$$

External inputs also come in as events $\tilde{e}_k \in \tilde{\mathbf{e}}$, $\tilde{e}_k = (s_k, i_k)$, where s_k are the continuous (real-valued) event times, and i_k denotes the index of the input component that got activated. Only the activations $a_{X,l}$ for the l -th unit experience a transition/jump on incoming external input events, as follows:

$$a_{X,l}^+(s_k) = a_{X,l}^-(s_k) + u_{X,ln_k} \times x_{i_k}(s_k), \quad (\text{S12})$$

where $x_{i_k}(s_k) = (\mathbf{x}(s_k))_{i_k}$ is the i_k -th component of the input \mathbf{x} at time s_k . The internal state \mathbf{c} remains the same on the external input event. That is, $c_l^+ = c_l^-$.

Using basic matrix algebra, it can be shown that both $\frac{\partial F}{\partial \mathbf{c}}$ and $\frac{\partial F}{\partial \mathbf{a}_X}$ simplify to a diagonal matrix due to the independence of a notional unit i from unit j in the forward dynamics in Eqns. (3), (4). Therefore, Eqn. (8) can be written as the following for unit i :

$$\frac{\partial \dot{c}_i}{\partial c_i} \lambda_{c,i} - \tau_m \dot{\lambda}_{c,i} = 0, \quad \lambda_{a_x,i} + \frac{\partial \dot{c}_i}{\partial a_{X,i}} \lambda_{c,i} - \tau_s \dot{\lambda}_{a_x,i} = 0, \quad (\text{S13})$$

where $\dot{c}_i = (F)_{,i}$, the i th element of F .

C Derivation of event-based learning rule in continuous time

In this section we derive the event-based updates for the network weights. The update questions yield different results for the recurrent weights (\mathbf{V}_X), biases (\mathbf{b}_X) and input weights (\mathbf{U}_X), which are derived in the remainder of this section. To increase readability important terms are highlighted in color.

C.1 Gradient updates for the recurrent weights \mathbf{V}_X

We first split the integral Eq. (7) across events as:

$$\mathcal{L} = \sum_{k=0}^N \int_{s_k}^{s_{k+1}} \left[\ell_c(\mathbf{c}(t), t) + \lambda_c \cdot f_c + \sum_{X \in \{u,r,z\}} \lambda_{a_X} \cdot f_{a_X} \right] dt. \quad (\text{S14})$$

Then taking the derivative of the full loss function, we get:

$$\frac{d\mathcal{L}}{dv_{ji}} = \frac{d}{dv_{ji}} \left\{ \sum_{k=0}^N \int_{s_k}^{s_{k+1}} \left[\ell_c(\mathbf{c}(t), t) + \lambda_c \cdot f_c + \sum_{X \in \{u,r,z\}} \lambda_{a_X} \cdot f_{a_X} \right] dt \right\}. \quad (\text{S15})$$

By application of Leibniz integral rule we get,

$$\frac{d}{dv_{ji}} \int_{s_k}^{s_{k+1}} \ell_c(\mathbf{c}(t), t) dt = \ell_c(\mathbf{c}, s_{k+1}) \frac{ds_{k+1}}{dv_{ji}} - \ell_c(\mathbf{c}, s_k) \frac{ds_k}{dv_{ji}} + \int_{s_k}^{s_{k+1}} \frac{\partial \ell_c}{\partial \mathbf{c}} \cdot \frac{\partial \mathbf{c}}{\partial v_{ji}} dt. \quad (\text{S16})$$

and

$$\frac{d}{dv_{ji}} \int_{s_k}^{s_{k+1}} \lambda_c \cdot f_c dt \quad (\text{S17})$$

$$= \int_{s_k}^{s_{k+1}} \lambda_c \cdot \frac{df_c}{dv_{ji}} dt = \int_{s_k}^{s_{k+1}} \lambda_c \cdot \left\{ \tau_m \frac{d}{dt} \frac{\partial \mathbf{c}}{\partial v_{ji}} + \frac{\partial F}{\partial v_{ji}} \right\} dt \quad (\text{S18})$$

$$= \tau_m \left[\lambda_c \cdot \frac{\partial \mathbf{c}}{\partial v_{ji}} \right]_{s_k}^{s_{k+1}} \quad (\text{S19})$$

$$- \tau_m \int_{s_k}^{s_{k+1}} \left\{ \dot{\lambda}_c \cdot \frac{\partial \mathbf{c}}{\partial v_{ji}} + \lambda_c \cdot \left(\left(\frac{\partial F}{\partial \mathbf{c}} \right)^T \frac{\partial \mathbf{c}}{\partial v_{ji}} + \sum_{X \in \{u,r,z\}} \left(\frac{\partial F}{\partial \mathbf{a}_X} \right)^T \frac{\partial \mathbf{a}_X}{\partial v_{ji}} \right) \right\} dt, \quad (\text{S20})$$

where we first apply Gronwall's theorem [6], then integration by parts, and M^T denotes the transpose of matrix M . $\ell_c(\mathbf{c}(t), t)$ is the instantaneous loss evaluated at time t . Similarly,

$$\frac{d}{dv_{ji}} \int_{s_k}^{s_{k+1}} \sum_{x \in \{u, r, z\}} \lambda_{a_x} \cdot f_{a_x} dt = \sum_{x \in \{u, r, z\}} \int_{s_k}^{s_{k+1}} \lambda_{a_x} \cdot \left\{ \tau_s \frac{d}{dt} \frac{\partial \mathbf{a}_x}{\partial v_{ji}} + \frac{\partial \mathbf{a}_x}{\partial v_{ji}} \right\} dt \quad (\text{S21})$$

$$= \tau_s \left[\lambda_{a_x} \cdot \frac{\partial \mathbf{a}_x}{\partial v_{ji}} \right]_{s_k}^{s_{k+1}} - \tau_s \int_{s_k}^{s_{k+1}} \left\{ \dot{\lambda}_{a_x} \cdot \frac{\partial \mathbf{a}_x}{\partial v_{ji}} + \lambda_{a_x} \cdot \frac{\partial \dot{\mathbf{a}}_x}{\partial v_{ji}} \right\} dt, \quad (\text{S22})$$

since $\frac{\partial \mathbf{b}}{\partial v_{ji}} = 0$.

Substituting these values into Eq. (S15), and setting the coefficients of terms with $\frac{\partial \mathbf{c}}{\partial v_{ji}}$ and $\frac{\partial \mathbf{a}_x}{\partial v_{ji}}$ to zero (using the fact that we can choose the adjoint variables freely due to f_c and f_{a_x} being everywhere zero by definition), we get the dynamics of the adjoint variable described in Eq. (8). The adjoint variable is usually integrated backwards in time starting from $t = T$, also due to its dependence on the loss values. The initial conditions for the adjoint variables is defined as $\lambda_c = \lambda_{a_x} = \mathbf{0}$.

Setting the coefficients of terms with $\frac{\partial \mathbf{c}}{\partial v_{ji}}$ and $\frac{\partial \mathbf{a}_x}{\partial v_{ji}}$ to zero allows us to write the parameter updates as:

$$\frac{d\mathcal{L}}{dv_{ji}} = \sum_{k=0}^N \left\{ (l_c^- - l_c^+) \frac{ds}{dv_{ji}} + \tau_s \sum_x \left(\lambda_{a_x}^- \cdot \frac{\partial \mathbf{a}_x^-}{\partial v_{ji}} - \lambda_{a_x}^+ \cdot \frac{\partial \mathbf{a}_x^+}{\partial v_{ji}} \right) + \tau_m \left(\lambda_c^- \cdot \frac{\partial \mathbf{c}^-}{\partial v_{ji}} - \lambda_c^+ \cdot \frac{\partial \mathbf{c}^+}{\partial v_{ji}} \right) \right\} \quad (\text{S23})$$

$$= \sum_{k=0}^N \xi_{X,ijk} \quad (\text{S24})$$

To define the required jumps at event times for the adjoint variables, we start with finding the relationship between $\frac{\partial \mathbf{c}^-}{\partial v_{ji}}$ and $\frac{\partial \mathbf{c}^+}{\partial v_{ji}}$. Eqs. (S7) define s_k as a differentiable function of v_{ji} under the condition $\dot{c}_{n_k}^- \neq 0$ and $\dot{c}_{n_k}^+ \neq 0$ due to the implicit function theorem [20, 21].

$$c_{n_k}^- - \vartheta_{n_k} = 0 \quad (\text{S25})$$

$$\frac{\partial c_{n_k}^-}{\partial v_{ji}} + \frac{dc_{n_k}^-}{ds} \frac{\partial s}{\partial v_{ji}} = 0 \quad (\text{S26})$$

$$\frac{\partial c_{n_k}^-}{\partial v_{ji}} + \dot{c}_{n_k}^- \frac{\partial s}{\partial v_{ji}} = 0 \quad (\text{S27})$$

$$\frac{\partial s}{\partial v_{ji}} = \frac{-1}{\dot{c}_{n_k}^-} \frac{\partial c_{n_k}^-}{\partial v_{ji}}, \quad (\text{S28})$$

where we write $\frac{dc_{n_k}^-}{ds} \equiv \dot{c}_{n_k}^-$ and $\dot{c}_{n_k}^- \neq 0$. Similarly,

$$c_{n_k}^+ = 0 \quad (\text{S29})$$

$$\frac{\partial c_{n_k}^+}{\partial v_{ji}} + \dot{c}_{n_k}^+ \frac{\partial s}{\partial v_{ji}} = 0 \quad (\text{S30})$$

which allows us to write

$$\frac{\partial c_{n_k}^+}{\partial v_{ji}} = \frac{\dot{c}_{n_k}^+}{\dot{c}_{n_k}^-} \frac{\partial c_{n_k}^-}{\partial v_{ji}} \quad (\text{S31})$$

Similarly, starting from $c_m^+ = c_m^-$, we can derive

$$\frac{\partial c_m^+}{\partial v_{ji}} = \frac{\partial c_m^-}{\partial v_{ji}} - \frac{1}{\dot{c}_{n_k}^-} \frac{\partial c_{n_k}^-}{\partial v_{ji}} (\dot{c}_m^- - \dot{c}_m^+) \quad (\text{S32})$$

For the activations \mathbf{a}_x , we use Eqs. (S8)–(S11) to derive the relationships between $\frac{\partial a_x}{\partial v_{ji}}^+$ and $\frac{\partial a_x}{\partial v_{ji}}^-$. Thus, we have:

$$\frac{\partial a_{x,m}^+}{\partial v_{ji}} = \frac{\partial a_{x,m}^-}{\partial v_{ji}} - \frac{1}{\tau_s} \frac{v_{mn_k} r_{x,n_k}^- c_{n_k}^-}{\dot{c}_{n_k}^-} \frac{\partial c_{n_k}^-}{\partial v_{ji}} + \delta_{in_k} \delta_{jm} c_{n_k}^- + c_{n_k}^- v_{mn_k} \frac{\partial r_{x,n_k}^-}{\partial v_{ji}} - c_{n_k}^- v_{mn_k} \frac{\dot{r}_{x,n_k}^-}{\dot{c}_{n_k}^-} \frac{\partial c_{n_k}^-}{\partial v_{ji}} \quad (\text{S33})$$

$$\frac{\partial a_{x,n_k}^+}{\partial v_{ji}} = \frac{\partial a_{x,n_k}^-}{\partial v_{ji}} \quad (\text{S34})$$

where $\mathbf{r}_x = \mathbf{0}$ if $x \in \{u, r\}$ and $\mathbf{r}_x = \mathbf{r}$ if $x = \{z\}$.

Substituting Eqs. (S31), (S32), (S34), (S33) into Eq. (S23), we get:

$$\xi_{x,ijk} = \left\{ \frac{\partial c_{n_k}^-}{\partial v_{ji}} \left(\frac{-1}{\dot{c}_{n_k}^-} (\ell_c^+ - \ell_c^-) + \tau_m \left(\lambda_{c,n_k}^- - \frac{\dot{c}_{n_k}^+}{\dot{c}_{n_k}^-} \lambda_{c,n_k}^+ \right) + \tau_m \frac{1}{\dot{c}_{n_k}^-} \sum_{m \neq n_k} \lambda_{c,m}^+ (\dot{c}_m^- - \dot{c}_m^+) \right) \right. \quad (\text{S35})$$

$$\left. + \sum_x \frac{r_{x,n_k}^- c_{n_k}^-}{\dot{c}_{n_k}^-} \sum_{m \neq n_k} v_{mn_k} \lambda_{a_x,m}^+ + \tau_s \sum_x \frac{\dot{r}_{x,n_k}^- c_{n_k}^-}{\dot{c}_{n_k}^-} \sum_{m \neq n_k} v_{mn_k} \lambda_{a_x,m}^+ \right) \quad (\text{S36})$$

$$+ \tau_m \sum_{m \neq n_k} \frac{\partial c_m^-}{\partial v_{ji}} (\lambda_{c,m}^- - \lambda_{c,m}^+) \quad (\text{S37})$$

$$\tau_s \sum_x \frac{\partial a_{x,n_k}^-}{\partial v_{ji}} \left((\lambda_{a_x,n_k}^- - \lambda_{a_x,n_k}^+) - c_{n_k}^- G'(a_{x,n_k}^-) \sum_{m \neq n_k} v_{mn_k} \lambda_{a_x,m}^+ \right) \quad (\text{S38})$$

$$\tau_s \sum_x \sum_{m \neq n_k} \frac{\partial a_{x,m}^-}{\partial v_{ji}} (\lambda_{a_x,m}^- - \lambda_{a_x,m}^+) \quad (\text{S39})$$

$$\left. - \tau_s \delta_{in_k} r_{x,n_k}^- c_{n_k}^- \sum_{m \neq n_k} \delta_{jm} \lambda_{a_x,m}^+ \right\} \quad (\text{S40})$$

where we use $\mathbf{r}_x = G(\mathbf{a}_x)$ to denote $G(\mathbf{a}_r) = \mathbf{r}$ and $G(\mathbf{a}_z) = G(\mathbf{a}_u) = \mathbf{1}$, δ_{ab} is the kronecker delta defined as:

$$\delta_{ab} = \begin{cases} 1 & \text{if } a = b, \\ 0 & \text{otherwise} \end{cases} \quad (\text{S41})$$

Setting the coefficients of $\frac{\partial c^-}{\partial v_{ji}}$ and $\frac{\partial a_x^-}{\partial v_{ji}}$ to 0 (again, using our ability to choose the adjoint variables freely), we can get both $\xi_{x,ijk}$ and the transitions for the adjoint variables.

For the parameter updates we get:

$$\xi_{ijk} = -\tau_s \delta_{in_k} r_{x,n_k}^- c_{n_k}^- \sum_{m \neq n_k} \delta_{jm} \lambda_{a_x,m}^+ \quad (\text{S42})$$

$$= -\tau_s r_{x,i}^- c_i^- \lambda_{a_x,j}^+ \quad (\text{S43})$$

Thus we can write:

$$\Delta w_{x,ij} = \frac{\partial}{\partial w_{x,ij}} \mathcal{L}(\mathbf{W}) = \sum_k \xi_{x,ijk} \cdot \quad (\text{S44})$$

The corresponding value of $\xi_{x,ijk} = (\xi_{x,k})_{ij}$ is given by the following formula, written in vector form for succinctness:

$$\xi_{x,k} = -\tau_s (\mathbf{r}_x^-(s_k) \odot \mathbf{c}^-(s_k)) \otimes \lambda_{a_x}^+(s_k), \quad (\text{S45})$$

The jumps/transitions of the adjoint variables are:

$$\lambda_{a_x,m}^+ = \lambda_{a_x,m}^- \quad (\text{S46})$$

$$\lambda_{a_x,n_k}^+ = \lambda_{a_x,n_k}^- - c_{n_k}^- G'(a_{x,n_k}) \sum_{m \neq n_k} v_{mn_k} \lambda_{a_x,m}^+ \quad (\text{S47})$$

$$\lambda_{c,m}^+ = \lambda_{c,m}^- \quad (\text{S48})$$

$$\begin{aligned} \tau_m \dot{c}_{n_k}^+ \lambda_{c,n_k}^+ &= -(\ell_c^+ - \ell_c^-) + \tau_m \dot{c}_{n_k}^- \lambda_{c,n_k}^- + \tau_m \sum_{m \neq n_k} \lambda_{c,m}^+ (\dot{c}_m^- - \dot{c}_m^+) \\ &\quad + \tau_s c_{n_k}^- \sum_x \left(\dot{r}_{x,n_k}^- + \frac{r_{x,n_k}^-}{\tau_s} \right) \sum_{m \neq n_k} v_{mn_k} \lambda_{a_x,m}^+, \end{aligned} \quad (\text{S49})$$

where $(\ell_c^+ - \ell_c^-)$ denotes the jumps in the instantaneous loss around event time s_k . Thus, all the quantities on the right hand side of Eq. (S23) can be calculated from known quantities.

C.2 Gradient updates for biases \mathbf{b}_x

Proceeding similarly for the biases \mathbf{b}_x for each of $x \in \{u, r, z\}$ (dropping the subscript x for simplicity):

$$\frac{d\mathcal{L}}{db_i} = \frac{d}{db_i} \left\{ \sum_{k=0}^N \int_{s_k}^{s_{k+1}} \left[\ell_c(\mathbf{c}(t), t) + \lambda_c \cdot f_c + \sum_{x \in \{u, r, z\}} \lambda_{a_x} \cdot f_{a_x} \right] dt \right\}. \quad (\text{S50})$$

the $\xi_{x,ik}^{\text{bias}}$ term can be shown to be:

$$\xi_{x,ik}^{\text{bias}} = \int_{s_k}^{s_{k+1}} \lambda_{a_x,i} dt \quad (\text{S51})$$

with

$$\frac{d\mathcal{L}}{db_i} = \sum_{k=0}^N \xi_{x,ik}^{\text{bias}}. \quad (\text{S52})$$

C.3 Gradient updates for input weights \mathbf{U}_x

Proceeding similarly for the input weights \mathbf{U}_x for each of $x \in \{u, r, z\}$ (dropping the subscript x for simplicity):

$$\frac{d\mathcal{L}}{du_{jx}} = \frac{d}{du_{jx}} \left\{ \sum_{k=0}^N \int_{s_k}^{s_{k+1}} \left[\ell_c(\mathbf{c}(t), t) + \lambda_c \cdot f_c + \sum_{x \in \{u, r, z\}} \lambda_{a_x} \cdot f_{a_x} \right] dt \right\}. \quad (\text{S53})$$

the $\xi_{x,jxk}^{\text{input}}$ term can be shown to be:

$$\xi_{x,jxk}^{\text{input}} = -\tau_s \lambda_{a_x,j}^+ x_x \quad (\text{S54})$$

with

$$\frac{d\mathcal{L}}{du_{jx}} = \sum_{k=0}^N \xi_{x,jxk}^{\text{input}}. \quad (\text{S55})$$

D Details of experiments

D.1 DVS128 Gesture recognition

In this experiment we use Tonic library [11] to prepare the dataset. The recordings in the dataset are sliced by time without any overlap to produce samples of length 1.7 seconds. The data is denoised

with a filter time of 10ms and normalised to [0;1] before being fed to the model. The positive and negative polarity events are represented by 2 separate channels. Our model consists of a preprocessing layer which performs downscaling and flattening transformations, followed by two RNN layers. Both RNN layers have the same number of hidden dimensions. Finally, a fully connected layer of size 11 performs the classification. All the weights were initialised using Xavier uniform distribution, while the biases were initialised using a uniform distribution. The unit thresholds were initialised using a normal distribution with mean 0 and standard deviation of $\sqrt{2}$, but was transformed to their absolute value after every update. We use cross-entropy loss and Adam optimizer with default parameters (0.001 learning rate, $\beta_1 = 0.9$, $\beta_2 = 0.999$). The learning rate is scaled by 80% every 100 epochs.

We use additional loss to regularize the output and increase sparsity of the network. The applied regularization losses are shown in Eq. (S57). L_{reg} is applied indirectly to the active outputs and L_{act} is applied on the auxiliary internal state $c_i^{(t)}$, the threshold parameter ϑ_i is detached from the graph in the second equation so the loss only affects the internal state. We set the regularization weights w_{reg} and w_v to 0.01 and 0.05 respectively.

Fig. S2(a) shows comparison of training curves for LSTM, GRU and EGRU, mean activity of the EGRU network is also shown, the network achieved 80%+ sparsity without significant drop in accuracy. The activities of LSTM and GRU are not shown in Fig S2(a) since they are always 100%. In our experiments we calculate sparsity of these networks as average number of activations close to zero with an absolute tolerance of 1×10^{-8} , however in Fig. S2(b) we show that even if we increase the absolute tolerance to 1×10^{-3} , the sparsity of these networks is still an order of magnitude lower than EGRU.

Hyperparameters were chosen by conducting a grid search over the number of units (32 - 2048), number of layers (1 - 4) and values of regularization weights. Learning rate and optimizer was chosen from initial experiments. Since batch size did not have any significant effect on training, we chose a batch size that maximizes GPU utilization. Models with CNN feature extractors are trained with slightly different hyper-parameters than the pure RNNs. These hyperparameters are chosen by a Bayesian search. This includes hidden to hidden dropout p_h of 0.4 for CNN+EGRU(256) and 0.08 for CNN+EGRU(795). The batch size used in this case is 40 to ease data augmentation. The learning rate is set initially to 0.001 and then scaled by 80% every 60 epochs. The input channels are combined into a single channel by averaging over the channel dimension.

$$L_{reg} = w_{reg} \left(\frac{1}{N} \frac{1}{n_{\text{units}}} \sum_{n=1}^N \sum_{i=1}^{n_{\text{units}}} H \left(c_i^{(t)} - \vartheta_i \right) - 0.05 \right) \quad (\text{S56})$$

$$L_{act} = w_v \left(\frac{1}{N} \frac{1}{n_{\text{units}}} \sum_{n=1}^N \sum_{i=1}^{n_{\text{units}}} c_i - (\vartheta_i - 0.05) \right) \quad (\text{S57})$$

where N spans mini-batch.

D.1.1 Ablation study

We performed ablation studies, showing the performance of the EGRU models with variation of the gating mechanism. All models in this study are a variation of our **EGRU**(1024) model. The results of these experiments are presented in Table S6. By using a scalar threshold ϑ where all units share a same threshold parameter we find that the accuracy drops by 2% but the the activity sparsity is increased to 90%.

Next, we evaluate a model with ‘hard reset’ where the auxiliary internal state $c_i^{(t)}$ is set to 0 every time an event is emitted by an unit. We observe a drop in accuracy possibly because the hard reset loses information when the internal state has gone above threshold at at any particular simulation time step, which may happen due to the limitations on precision in discrete time simulations with a fixed time grid. This drop in performance might be significant for applications which require high temporal resolution, which necessitates the term $-y_i^{(t-1)}$ in Eq. (2). Model is also evaluated with ‘no reset’ where the term $-y_i^{(t-1)}$ is removed from Eq. (2) which results in slightly lower accuracy and sparsity.

input size (# bits)	network size (# units)	delay (time)	iterations to convergence (mean \pm std)
2	2	2	15.0 \pm 8.9
2	2	3	10.0 \pm 5.3
2	5	2	16.0 \pm 13.3
3	32	2	17 \pm 11.0
3	32	5	28.3 \pm 23.8

Table S1: Model performance of continuous time EGRU trained using hybrid continuous/discrete adjoint method for different parameter values. Performance reported as number of iterations to reach perfect bitwise accuracy (100%) on this task. Mean and standard deviation over 3 runs are reported.

delay (steps)	GRU	EGRU
2	87.6 \pm 1.7	240.3 \pm 22.7
4	128.0 \pm 11.4	451.0 \pm 99.8
8	321.0 \pm 76.9	841.6 \pm 132.5
16	1034.6 \pm 210.0	1755.0 \pm 158.3

Table S2: Comparing memory capacity of the GRU and the discrete-time EGRU on the delay copy task. The binary pattern used is 3 bits wide and 2 bits long, given to a network with 256 units in all rows with a batch size of 1000. Performance reported as number of iterations to reach 98% bitwise accuracy on this task. Mean and standard deviation over 3 runs are reported.

architecture (# units)	para- meters	effective MAC (mean \pm std)	accu- racy (%) (mean \pm std)	activity sparsity (%) (mean \pm std)	backward sparsity (%) at epoch 100 (mean \pm std)
LSTM (867)	16.28M	20.97M	87.9 \pm 1.0	0	-
GRU (1024)	15.75M	15.73M	88.1 \pm 0.8	0	-
EGRU (512)	5.51M	4.31M \pm 93.14K	86.0 \pm 1.2	76.1 \pm 5.9	45.7 \pm 0.7
EGRU (1024)	15.75M	10.71M \pm 206.05K	87.7 \pm 2.1	79.8 \pm 3.3	54.4 \pm 1.2
EGRU (1024)*	110.12M	105.24M \pm 441.30K	85.7 \pm 0.9	77.3 \pm 7.0	64.6 \pm 1.1
CNN+EGRU (256)*	1.7M+1.0M**	0.69M \pm 8.30K \dagger	96.8 \pm 0.3	73.3 \pm 2.1	55.2 \pm 1.3
CNN+EGRU (795)*	1.7M+3.1M**	1.65M \pm 34.29K \dagger	97.3 \pm 0.4	77.6 \pm 1.8	72.7 \pm 1.0

Table S3: Model performance over 5 runs for the DVS Gesture recognition task. Effective number of MAC operations as described in section 3.5. * indicates network with 128×128 input size, all other networks have scaled input as explained in Section 4.2. ** Indicated parameters are split between CNN and RNN. \dagger Only RNN MAC operations. CNN adds additional 7.9M parameters, however since these are not affected by activity sparsity, we exclude them from this table for brevity.

layer	channels	output shape
Input	1	128x128
Convolution	64	31x31
ReLU	64	31x31
Pooling	64	15x15
Convolution	192	15x15
ReLU	192	15x15
Pooling	192	7x7
Convolution	384	7x7
ReLU	384	7x7
Pooling	384	3x3
Convolution	256	3x3
ReLU	256	3x3
Pooling	256	1x1
Convolution	256	1x1
ReLU	256	1x1
Fully connected	512	1x1
ReLU	512	1x1

Table S4: Details of CNN layers for the feature extraction head used in CNN+EGRU models

Model	EGRU	CNN+EGRU	CNN+EGRU
Hidden units	512/1024	795	256
Layers	2	1	2
Learning rate	0.001	0.001	0.001
Learning rate decay	0.8	0.874	0.8
Learning rate decay epochs	100	56	100
Batch size	256	40	40
Dropout p_l	0	0.632	0
DropConnect p_h	0	0.081	0.4
Zoneout p_z	0	0.2	0
Activity regularization	0.01	0.01	0.01
Surrogate gradient ϵ	1	0.588	1
Threshold init μ	0	-0.246	0

Table S5: Detailed hyper-parameters of our best models for DVS Gesture recognition.

model	accuracy (%)	activity sparsity (%)
Full EGRU (1024)	90.2	82.5
without regularization	89.3	76.5
scalar ϑ	88.3	90.8
hard reset	87.2	90.0
no reset	88.9	80.7

Table S6: Performance of the EGRU (1024) model for the ablation study performed on the DVS gesture task as described in Section D.1.1.

D.2 Sequential MNIST

All the weights were initialised using Xavier uniform distribution, while the biases were initialised using a uniform distribution. The unit thresholds were initialised using a normal distribution with mean 0 and standard deviation of $\sqrt{2}$, but was transformed to be between 0 and 1 by passing through a standard sigmoid/logistic function after every update. We used a batch size of 500 for sMNIST and 300 for psMNIST. In all the experiments, we trained the network with Adam with default parameters (0.001 learning rate, $\beta_1 = 0.9$, $\beta_2 = 0.999$) on a cross-entropy loss function. We used gradient clipping with a max gradient norm of 0.25. We trained models for 200 epochs for sMNIST and 700 epochs for psMNIST. The model trained on psMNIST used DropConnect [19] with $p = 0.4$. The outputs of all the units were convolved with an exponential filter with time constant of 10 time units i.e. with $e^{-\frac{1}{10}}$ to calculate an output trace. The value of this trace at the last time step was used to predict the class through a softmax function.

For sMNIST, hyper-parameters were chosen by performing a search over batch sizes (50-1000), learning rates (10^{-3} , 10^{-4}), use of output trace, activity regularisation. An extensive Bayesian search was conducted using Weights & Biases [2] to optimize hyperparameters of EGRU with 590 hidden units on psMNIST on NVIDIA V100 GPUs. The initialisation method of the thresholds were also tweaked – currently we use a normal initialisation with a sigmoid projection into the $[0, 1]$ range, but we experimented with projecting it with an absolute value followed by clipping, which proved unstable.

D.3 PTB Language modeling

Our experimental setup largely follows [15]. In particular, we download and preprocess PennTreebank [12] and WikiText-2 [14] with their published code¹. Words are projected to an d_{emb} -dimensional dense vector by a linear transformation, followed by three RNN layers without skip connections. The first two RNN layers feature the same hidden dimension, while the hidden dimension of the last RNN layer equals the word vector embedding dimension. As common in language modeling, we apply cross entropy loss and use weight tying [7, 18].

D.3.1 Training details and hyperparameter optimization

Our activity sparsity mechanism introduces two new hyperparameters ϵ and μ . First, the shape of the surrogate gradient

$$\frac{dH}{dc} = \lambda \max(1 - |c|/\epsilon) \quad (\text{S58})$$

is defined by ϵ , which thus determines the backward sparsity. Second, the initialization of the rectifier thresholds φ determines both inference and BPTT sparsity at initialization. We choose to reparameterize thresholds with a sigmoid function to limit their domain to the interval $[0, 1]$. With τ_i drawn from a normal distribution $\tau_i \sim \mathcal{N}(\mu, \sqrt{2})$, the thresholds are initialized as $\varphi_i = 1/(1 + \exp(-\tau_i))$, where τ_i are the trainable parameters and μ is the new hyperparameter.

We apply most of the regularization strategies of [15], except for (temporal) activity regularization. Backpropagation through time is conducted with a variable sequence length. With 95% probability, the sequence length is drawn from $\mathcal{N}(s, 5)$, and with 5% probability the sequence length is drawn from $\mathcal{N}(s/2, 5)$, where s is a tuned hyperparameter. We apply variational dropout [5] to the vocabulary with probability p_{voc} , to the word embedding vectors with probability p_{emb} as well as to each layer output with probability p_l . DropConnect [19] was applied to the hidden-to-hidden weight matrices with probability p_h . We experimented with both Adam [8] and NT-AvSGD [15] optimization procedures. While Adam lead to competitive results for all models, GRU based models did not converge to competitive results using NT-AvSGD. When optimized with SGD based optimizers, both GRU and EGRU fell behind Adam optimized models. Momentum was set to 0 as reported in [13]. Gradient clipping was applied to all models, where the magnitude of clipped gradients only made very small differences in results. While gradient clipping of 0.25 was used for GRU, we used 2.0 for EGRU.

We apply a cosine-annealing learning rate schedule, where the first $n/2$ epochs were trained at constant learning rate λ , and a cosine decay from λ to $0.1 \cdot \lambda$ was applied for the remaining $n/2$ epochs. All EGRU models were trained for 2500 epochs.

¹<https://github.com/salesforce/awd-lstm-lm>

An extensive Bayesian search was conducted using Weights & Biases [2] to optimize hyperparameters of GRU with 1350 hidden units and EGRU with 1350 and 2000 hidden units on Penn Treebank for about 65 GPU days on NVIDIA A100 GPUs. The surrogate gradient parameter ϵ and the initialization of the thresholds φ_i are treated as hyperparameters of this model. Due to our constrained computational resources, we used the same hyperparameters on WikiText-2.

We found the word embedding dimension $d_{\text{emb}} = 400$ set by [15] to be a good fit for GRU. For EGRU, we observed much larger dimensions around $d_{\text{emb}} = 800$ to outperform smaller dimensions. We hypothesize that the observed activation sparsity in the last layer of about 60% accounts for a similar expressivity of word embeddings between GRU and EGRU. See table S8 for detailed hyperparameters of the best models.

D.4 Model compression through activity pruning

We present a simple model compression heuristic based on activity. Starting from a trained model, we remove the least active r_i % of the units of layer i . Since we observed different levels of activity in the layers, we work with different combinations of compression rates r_i per layer. Figure S5 shows how model performance and sparsity depend on the model compression. Surprisingly, we observe very similar sparsity levels across the evaluated compressed models.

E Dataset licenses

Penn Treebank [12] is subject to the Linguistic Data Consortium User Agreement for Non-Members².

LDC Not-For-Profit members, government members and nonmember licensees may use LDC data for noncommercial linguistic research and education only. For-profit organizations who are or were LDC members may conduct commercial technology development with LDC data received when the organization was an LDC for-profit member unless use of that data is otherwise restricted by a corpus-specific license agreement. Not-for-profit members, government members and nonmembers, including nonmember for-profit organizations, cannot use LDC data to develop or test products for commercialization, nor can they use LDC data in any commercial product or for any commercial purpose.

Following [15], we download Penn Treebank data from <http://www.fit.vutbr.cz/~imikolov/rnnlm/simple-examples.tgz>.

The DVS128 Gesture Dataset [1] is released under the Creative Commons Attribution 4.0 license and can be retrieved from: <https://research.ibm.com/interactive/dvsgesture/>. We used Tonic library [11] for Pytorch to preprocess data and to apply transformations.

The sequential MNIST task [9] is based on the MNIST dataset first introduced in [10], available from: <http://yann.lecun.com/exdb/mnist/>.

F Hardware and software details

We implement EGRU as a modification of Haste GRU [16] and observe slightly shorter wallclock times than PyTorch’s [17] GRU implementation.

Most of our experiments were run on NVIDIA A100 GPUs. Some initial hyper-parameter searches were conducted on NVIDIA V100 and Quadro RTX 5000 GPUs. We used about 45,000 computational hours in total for training and hyper-parameter searches. All models and experiments were implemented in PyTorch. For the continuous time EGRU model, we also used the torchdiffeq [3] library.

The machines used for the DVS128 gesture recognition task and for the PTB language modeling task feature 8x NVIDIA A100-SXM4 (40GB) GPUs, 2x AMD EPYC CPUs 7352 with 24 cores each, and 1TB RAM on each compute node. For each run, we only use a single GPU, and a fraction of the cores and memory available on the node to run multiple experiments in parallel. The nodes operate Red Hat Enterprise Linux Server (release 7.9).

²<https://www ldc.upenn.edu/data-management/using/licensing>

architecture (# units)	parameters	effective MAC (mean±std)	test accuracy (%) (mean±std)	activity sparsity (%) (mean±std)	backwards sparsity (%) at epochs 20/50/100 (mean±std)
GRU (512)	791K	795K	98.6±0.2	-	-
GRU (590)	1.049M	1.054M	98.7±0.1	-	-
EGRU (512)	790K	(147±7)K	87.2±3.0	82.1±0.9	22.2±2.8/24.9±0.7/ 28.7± 1.1
EGRU (590)	1.048M	(210±51)K	95.5±1.6	80.5±4.9	24.9±6.8 / 26.1±5.9 / 25.6±1.7

Table S7: Model performance over 4 runs for sequential MNIST task. Test scores are given as percentage accuracy, where higher is better.

Model	GRU	EGRU	EGRU
Hidden units	1350	1350	2000
PTB			
Test ppl (best)	66.3	58.7	58.8
Val perplexity (best)	68.7	59.5	59.6
Val perplexity (best)	68.7	59.5	59.6
Forward sparsity (test)	(0.0 ± 0.0) %	(79.9 ± 0.1) %	(85.3 ± 0.9) %
Backward sparsity (train)	(0.0 ± 0.0) %	(46.0 ± 0.3) %	(40.5 ± 3.8) %
Effective MACs (RNN + emb)	(21.9 + 5.6) M	(6.8 + 3.1) M	(9.7 + 3.0) M
WT2			
Test perplexity (best)	71.8	70.6	68.9
Val perplexity (best)	75.7	73.9	71.5
Val ppl (mean ± std)	75.9 ± 0.1	74.0 ± 0.1	75.7 ± 6.5
Forward sparsity (test)	(0.0 ± 0.0) %	(77.0 ± 0.1) %	(84.6 ± 2.9) %
Backward sparsity (train)	(0.0 ± 0.0) %	(43.8 ± 0.3) %	(36.1 ± 8.7) %
Effective MACs (RNN + emb)	(21.9 + 16.9) M	(7.4 + 10.1) M	(10.6 + 9.5) M
Learning rate	4.62×10^{-4}	4.44×10^{-4}	4.94×10^{-4}
Batch size	96	64	128
Sequence length s	34	68	67
Embedding dimension d_{emb}	563	788	786
Dropout p_h	0.506	0.679	0.621
Dropout p_l	0.474	0.264	0.241
Dropout p_{emb}	0.729	0.707	0.765
Dropout p_{voc}	0.093	0.055	0.149
Weight decay	4.60×10^{-6}	9.01×10^{-6}	6.69×10^{-6}
Activity regularization	2.766	0	0
Temporal Activity regularization	0.29	0	0
Surrogate gradient ϵ	-	0.459	0.425
Threshold init μ	-	-3.769	-3.496

Table S8: Detailed results and parameters for our best models. Mean and standard deviations are calculated over 5 runs with different random seeds. Effective MAC operations consider the layer-wise sparsity in the forward pass. Activity sparsity is given for the trained model to resemble inference sparsity. Backward sparsity is averaged over the whole training. Model parameters were optimized on Penn Treebank and transferred to WikiText-2.

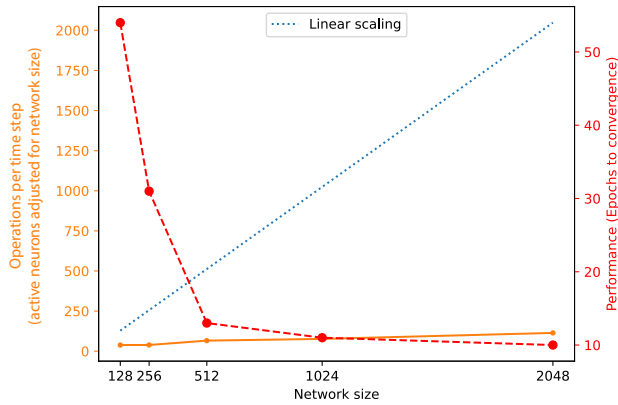


Figure S1: Illustration of the scaling properties of the EGRU on a 14×14 sequential MNIST task (1 run per network size). As the size of the network increases, the network converges faster. Increasing the network size 10x increases the speed of convergence 5x, while increasing the total amount of computation per sample only 2x. The total amount of computation is adjusted for network size. The smaller subsampled 14×14 sMNIST task was chosen here for reasons of computational limitations.

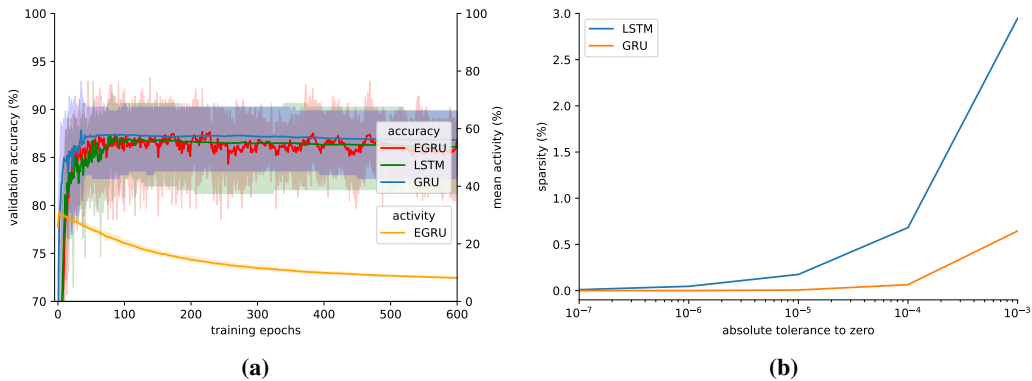


Figure S2: (a) mean training curves over 5 runs for DVS gesture task. (b) activity sparsity of LSTM and GRU for DVS gesture task over 1 run across various values of absolute tolerance to zero.

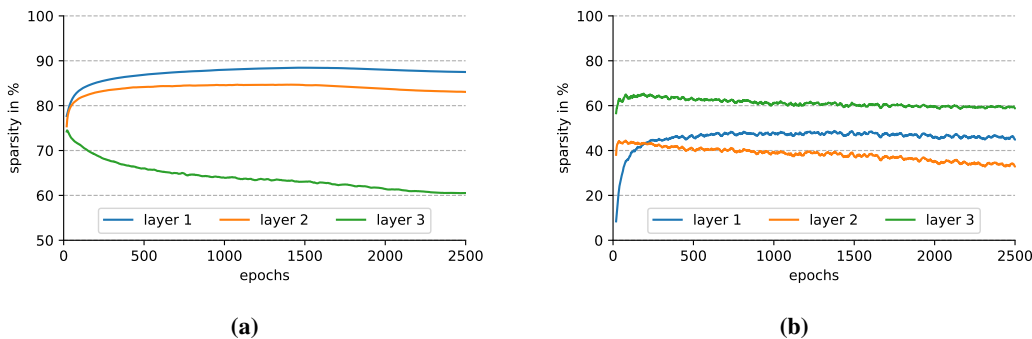


Figure S3: EGRU with 1350 hidden units on the Penn Treebank language modeling task with pseudo-derivative $\epsilon = 0.45$. (a) layer-wise forward sparsity (b) layer-wise backward sparsity

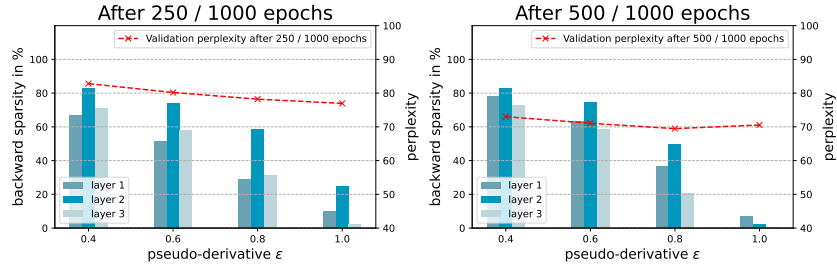


Figure S4: Backward sparsity and corresponding perplexity for a 3-layer EGRU with 1350 hidden units on the Penn Treebank language modeling task with varying pseudo-derivative support ϵ . Standard deviations are calculated over three runs with different random seeds.

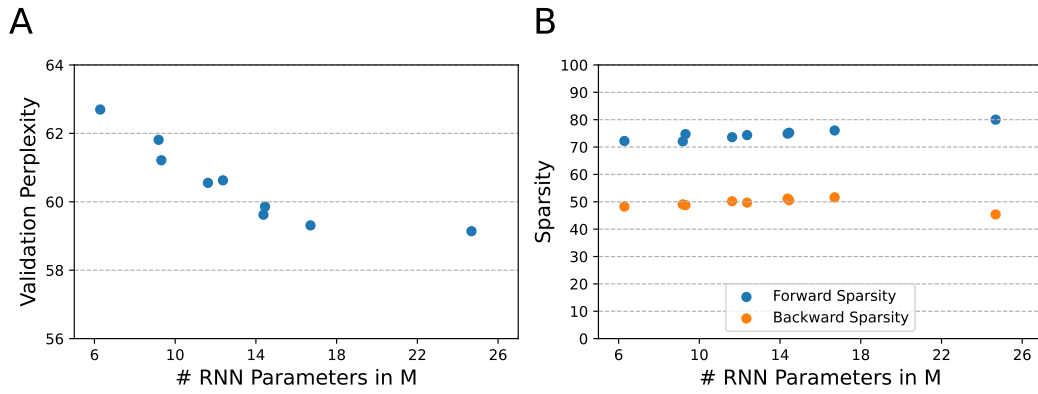


Figure S5: We apply different levels of layer-wise model compression according to Sec. D.4. **A** Model performance **B** Forward and backward sparsity

References

- [1] A. Amir, B. Taba, D. Berg, T. Melano, J. McKinstry, C. Di Nolfo, T. Nayak, A. Andreopoulos, G. Garreau, M. Mendoza, et al. A low power, fully event-based gesture recognition system. In *Proceedings of the IEEE conference on computer vision and pattern recognition*, pages 7243–7252, 2017.
- [2] L. Biewald. Experiment tracking with weights and biases, 2020. URL <https://www.wandb.com/>. Software available from wandb.com.
- [3] R. T. Q. Chen, Y. Rubanova, J. Bettencourt, and D. K. Duvenaud. Neural Ordinary Differential Equations. In S. Bengio, H. Wallach, H. Larochelle, K. Grauman, N. Cesa-Bianchi, and R. Garnett, editors, *Advances in Neural Information Processing Systems 31*, pages 6572–6583. Curran Associates, Inc., 2018.
- [4] K. Cho, B. Van Merriënboer, C. Gulcehre, D. Bahdanau, F. Bougares, H. Schwenk, and Y. Bengio. Learning phrase representations using rnn encoder-decoder for statistical machine translation. *arXiv preprint arXiv:1406.1078*, 2014.
- [5] Y. Gal and Z. Ghahramani. A theoretically grounded application of dropout in recurrent neural networks. In D. Lee, M. Sugiyama, U. Luxburg, I. Guyon, and R. Garnett, editors, *Advances in Neural Information Processing Systems*, volume 29. Curran Associates, Inc., 2016. URL <https://proceedings.neurips.cc/paper/2016/file/076a0c97d09cf1a0ec3e19c7f2529f2b-Paper.pdf>.
- [6] T. H. Gronwall. Note on the derivatives with respect to a parameter of the solutions of a system of differential equations. *Annals of Mathematics*, pages 292–296, 1919.
- [7] H. Inan, K. Khosravi, and R. Socher. Tying word vectors and word classifiers: A loss framework for language modeling. In *5th International Conference on Learning Representations, ICLR 2017, Toulon, France, April 24-26, 2017, Conference Track Proceedings*. OpenReview.net, 2017. URL <https://openreview.net/forum?id=r1aPbsFle>.
- [8] D. P. Kingma and J. Ba. Adam: A method for stochastic optimization. In Y. Bengio and Y. LeCun, editors, *3rd International Conference on Learning Representations, ICLR 2015, San Diego, CA, USA, May 7-9, 2015, Conference Track Proceedings*, 2015. URL <http://arxiv.org/abs/1412.6980>.
- [9] Q. V. Le, N. Jaitly, and G. E. Hinton. A simple way to initialize recurrent networks of rectified linear units. *arXiv preprint arXiv:1504.00941*, 2015.
- [10] Y. LeCun, L. Bottou, Y. Bengio, and P. Haffner. Gradient-based learning applied to document recognition. *Proceedings of the IEEE*, 86(11):2278–2324, 1998.
- [11] G. Lenz, K. Chaney, S. B. Shrestha, O. Oubari, S. Picaud, and G. Zarrella. Tonic: event-based datasets and transformations., July 2021. URL <https://doi.org/10.5281/zenodo.5079802>. Documentation available under <https://tonic.readthedocs.io>.
- [12] M. P. Marcus, M. A. Marcinkiewicz, and B. Santorini. Building a large annotated corpus of english: The penn treebank. *Comput. Linguist.*, 19(2):313–330, jun 1993. ISSN 0891-2017.
- [13] G. Melis, C. Dyer, and P. Blunsom. On the state of the art of evaluation in neural language models. In *6th International Conference on Learning Representations, ICLR 2018, Vancouver, BC, Canada, April 30 - May 3, 2018, Conference Track Proceedings*. OpenReview.net, 2018. URL <https://openreview.net/forum?id=ByJHuTgA->.
- [14] S. Merity, C. Xiong, J. Bradbury, and R. Socher. Pointer sentinel mixture models, 2016. URL <https://arxiv.org/abs/1609.07843>.
- [15] S. Merity, N. S. Keskar, and R. Socher. Regularizing and Optimizing LSTM Language Models. *arXiv:1708.02182 [cs]*, Aug. 2017.
- [16] S. Nanavati. Haste: a fast, simple, and open rnn library. <https://github.com/lmnt-com/haste/>, Jan 2020.

- [17] A. Paszke, S. Gross, F. Massa, A. Lerer, J. Bradbury, G. Chanan, T. Killeen, Z. Lin, N. Gimelshein, L. Antiga, A. Desmaison, A. Kopf, E. Yang, Z. DeVito, M. Raison, A. Tejani, S. Chilamkurthy, B. Steiner, L. Fang, J. Bai, and S. Chintala. Pytorch: An imperative style, high-performance deep learning library. In H. Wallach, H. Larochelle, A. Beygelzimer, F. d'Alché-Buc, E. Fox, and R. Garnett, editors, *Advances in Neural Information Processing Systems 32*, pages 8024–8035. Curran Associates, Inc., 2019.
- [18] O. Press and L. Wolf. Using the output embedding to improve language models. In *Proceedings of the 15th Conference of the European Chapter of the Association for Computational Linguistics: Volume 2, Short Papers*, pages 157–163, Valencia, Spain, Apr. 2017. Association for Computational Linguistics. URL <https://aclanthology.org/E17-2025>.
- [19] L. Wan, M. Zeiler, S. Zhang, Y. Le Cun, and R. Fergus. Regularization of neural networks using dropconnect. In S. Dasgupta and D. McAllester, editors, *Proceedings of the 30th International Conference on Machine Learning*, volume 28 of *Proceedings of Machine Learning Research*, pages 1058–1066, Atlanta, Georgia, USA, 17–19 Jun 2013. PMLR. URL <https://proceedings.mlr.press/v28/wan13.html>.
- [20] T. C. Wunderlich and C. Pehle. Event-based backpropagation can compute exact gradients for spiking neural networks. *Scientific Reports*, 11(1):12829, June 2021. ISSN 2045-2322. doi: 10.1038/s41598-021-91786-z. URL <https://www.nature.com/articles/s41598-021-91786-z>.
- [21] W. Yang, D. Yang, and Y. Fan. A proof of a key formula in the error-backpropagation learning algorithm for multiple spiking neural networks. In *International Symposium on Neural Networks*, pages 19–26. Springer, 2014.